applied sciences

MDPI

Article

A Model of Information Visualization Interpretation

Michael G. Hilgers

Business and Information Technology Department, Kummer College of Innovation, Entrepreneurship, and Economic Development, Missouri University of Science and Technology, 106D Fulton Hall, 301 W. 14th St., Rolla, MO 65409, USA; hilgers@mst.edu; Tel.: +1-573-341-6484

Abstract: Since the groundbreaking work by Cleveland and McGill in 1984, studies have revealed the difficulties humans have extracting quantitative data from visualizations as simple as bar graphs. As a first step toward understanding this situation, this paper proposes a mathematical model of the interpretation effort of a bar graph using concepts drawn from eye tracking. First, three key areas of interest (AOIs) are identified, and fixations are modeled as random point clouds within the AOIs. Stochastic geometry is introduced via random triangles connecting fixations within the adjacent key visual regions. The so-called landmark methodology provides the basis for the probabilistic analysis of the constructed system. It is found that the random length of interest in a stochastic triangle has a noncentral chi distribution with a known mean. Unique to this model, in terms of previous landmark applications, is the inclusion of a correlation between fixations, which is justified by physiological studies of the eyes. This approach introduces several model parameters, such as the noncentrality parameter, variance of the fixation cloud, correlation between fixations, and a visualization scale. A detailed parametric analysis examining the dependence of the mean on these parameters is conducted. The paper ties this work to the visualization via a definition of the *expected visual measurement error*. An asymptotic analysis of the visual error is performed, and a simple expression is found to relate the expected visual measurement error to the key model parameters. From this expression, the influence these parameters have on a visualization's interpretation is considered.

Keywords: eye tracking; visualization; stochastic geometry

check for updates

Citation: Hilgers, M.G. A Model of Information Visualization Interpretation. *Appl. Sci.* **2024**, *14*, 6731. https://doi.org/10.3390/app14156731

Academic Editor: Thomas Hurtut

Received: 28 June 2024
Revised: 22 July 2024
Accepted: 26 July 2024
Published: 1 August 2024

Copyright: © 2024 by the authors. Licensee MDPI, Basel, Switzerland. This article is an open access article distributed under the terms and conditions of the Creative Commons Attribution (CC BY) license (https://creativecommons.org/licenses/by/4.0/).

1. Introduction

The visual display of quantitative data requires the viewer to decode numerical information from visual objects [1], as shown in Figure 1. As the volume and dimension of data increase, the associated visualizations become increasingly more complex [2], making the decoding process more challenging. Much attention has been given to the success or failure of the decoding process. Research agendas have had a variety of objectives and have utilized various methodologies. A discussion of topics relevant to this paper follows.

An information visualization communicates numeric data using objects such as lines, rectangles, bars, circles, and so forth [1]. Cleveland and McGill, in their classic work on graphical perception [3], studied how the viewer assigns numbers to these objects using their geometric properties of points, lengths, areas, and so forth. Their results were repeated and extended on a larger experimental scale using crowd sourcing on Amazon's Mechanical Turk platform by Heer and Bostock [4]. The systemic difference they found between the user-perceived value and the desired numeric value is called the "expected visual measurement error" in this paper, and modeling it is one of the goals.

All models are based on assumptions. In order to build ours, we need to clarify the situation and context in which the decoding occurs. This requires an understanding of how people approach a visualization to read it.

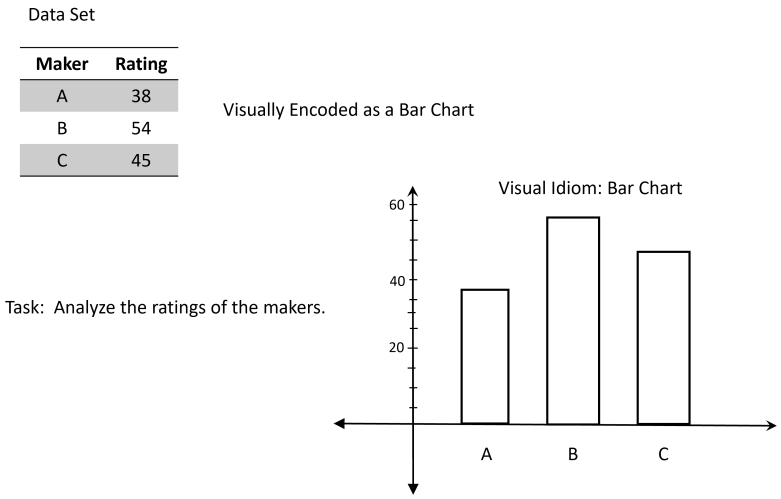


Figure 1. Conceptual structure of a simple bar graph. It shows the relationship between the table of data and the visual objects encoding it. The ruler is the key to the decoding process.

Shah and Hoeffner published a survey of graph comprehension research [5]. They found in the literature three major factors influencing a student's comprehension of graphs: visual characteristics of the graph, prior experience with visualizations, and knowledge and expectations with the content of the data in a graph. While measuring comprehension is not an objective of this research, it is assumed the viewer understands how to read a bar graph, which is not universally true.

Here we encounter a subtle point, which is the reason the viewer is inspecting the graph. Is the the person seeking an answer to a specific question, or is the viewer free to explore and deduce meaning? This introduces the concept of top-down versus bottom-up viewing of a visualization [6,7]. Top-down is goal-oriented, and visual attention is associated with the viewer's goals and expectations, whereas in bottom-up, visual attention is driven by the graphical characteristics of the image, such as color and contrast. Bottom-up is the free visual search. Matzen et al. have explored bottom-up situations in several studies using eye tracking [8,9]. This can be complicated due to the matter of memory. If the viewer is given a limited period to investigate the visualization, then memory must be used to fulfill a task [10]. In this paper, the concern is with a viewer who is given a specific task to fulfill, making this a top-down situation.

In moving from related cognitive issues to focus on the eye-tracking methodology, we find rich literature. Jacob and Karn [11] offer a detailed historical review of eye tracking starting in the 1800s. Much early research tried to tie eye tracking to the cognitive process. That is, how eye movement relates to the thought process [12–14]. A thread of recent research seeks to use eye tracking to discover how a viewer seeks out the salient features of the visualization [15]. This can be tied to visualization design via a so-called saliency map [8,16], which is used to predict user behavior. These maps are most applicable in a bottom-up situation.

Important to the use of eye-tracking data in the development of models is the capability to quantize it. The most common approach is through various metrics. In [11], 21 usability studies utilizing eye tracking were surveyed, and the metrics were classified and counted. Some of this is relevant herein. First, the concept of a fixation is needed. The authors defined it as follows [11]:

> "Fixation: A relatively stable eye-in-head position within some threshold of dispersion (typically 2°) over some minimum duration (typically 100–200 ms), and with a velocity below some threshold (typically 15–100 degrees per second)."

Next the concept of the area of interest (AOI) is needed, quoting [11]:

"Area of interest: Area of a display or visual environment that is of interest to the research or design team and thus defined by them (not by the participant)."

Finally, their notion of the scanpath is needed, so again quoting [11]:

"scanpath: Spatial arrangement of a sequence of fixations."

Acknowledged as an important metric [17], the scanpath contains information about the arrangement of elements in the image being viewed.

Eye tracking has also been used to study the physical motion of the eye during the reading of text or viewing of an image. Rather than give a complete summary of all that is known in this interesting area, attention is restricted to differences between horizontal and vertical motion of the eye and any potential correlation. Collewijn et al. studied these issues using eye tracking in a pair of papers [18,19]. It had already been established by Bahill and Stark that horizontal and vertical channels of eye movement are independent [20]. That is, there are different muscles, motor neurons, and brain stem staging areas controlling the two types of eye movements. The horizontal and vertical motions do not happen simultaneously so that an oblique scanpath is curved. Horizontal movement, with its associated saccadic behavior (rapid jumps), is dominant and more accurate. Vertical saccades are less accurate, often undershooting the target followed by a correction. Furthermore, parameters describing upward saccades are heavily depended on the position of the eye, while downward saccades are almost independent of eye position. Similarly, the authors found that the parametric dependence of horizontal motion is affected by the size, direction, and initial position of the motion.

Tying these threads to this paper, several observations are in order. The visualization under consideration will be a simple bar graph. It is assumed the viewer understands the graph and the underlying data structure. The visual characteristics of the graph are important. All elements are supposed to be of equal salience so that none draws unwarranted attention due to color or contrast. The viewer has a simple task to perform: determine the height of a particular bar using the y-axis (or ruler) provided. This makes for a top-down investigation. There is no time restriction that forces the viewer to rely on memory. In this stage of the model's development, the visual search factor is minimized by considering only one bar.

The developed model attempts to capture aspects of the physiological motion of the eyes using stochastic geometry. It is like the landmark theory by Bookstein [21]. However, it is a novel contribution to both eye tracking and applied stochastic geometry in that the random horizontal and vertical motions of the eye have different variances and are correlated. It should be noted that though the horizontal and vertical saccades are physiologically independent, they need not be statistically independent as suggested by the oblique [20] scanpaths that are often observed. Hence, the model is developed in its fullest generality; then, several examples under simplifying assumptions are examined.

The mathematical model is based on eye-tracking concepts in the following manner. A viewer is tasked with finding the numerical value associated with bar A. See Figure 2. The viewer must look at the base of the bar to identify it as the correct bar and to verify that its bottom aligns with the horizontal axis. The top of the bar is studied as part of the sighting process to match it with the associated location on the ruler. This defines three areas of interest. It should be noted that these three AOIs have been identified on bar graphs in other eye-tracking studies on information visualization [22]. During eye tracking, fixations occur in the AOIs. A type of mean case analysis is performed by assuming the fixations are normally distributed in the plane about the points $(b, 0)$, (b, h), and $(0, h)$. The nature of this normal distribution will be much discussed below. This is, of course, an abstraction of what happens in an eye-tracking experiment, but all of the results to follow will involve the mean of these fixations. Spatial statistics estimate this with the average of the fixation locations.

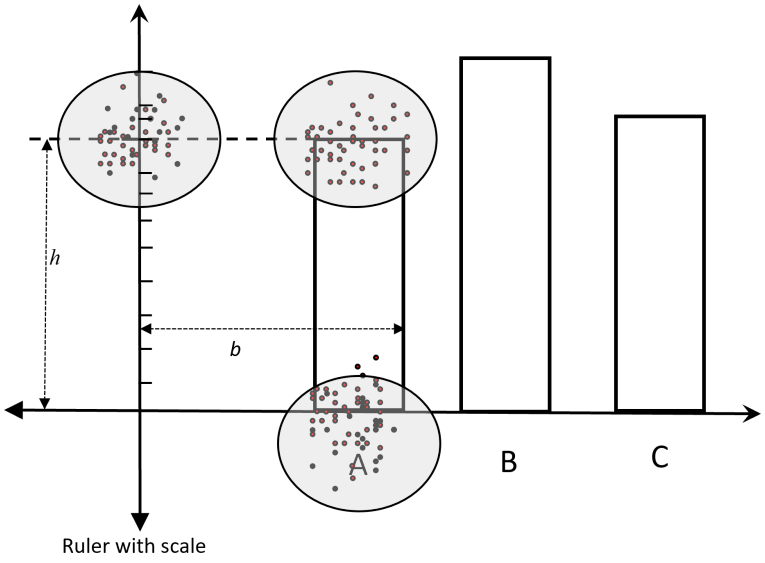


Figure 2. Conceptional view of the AOIs needed to read a bar graph. Each AOI contains fixations.

2. Materials and Methods

In this section, we will develop a model of eye tracking as applied to a bar graph, followed by extensive parametric analysis. Before this, we will consider the purpose and goals of parametric analysis. Once a sense of direction is established, we will construct the eye-tracking model in a general form. With this in hand, the model is examined under various restrictions that prove useful for a rich analysis of the errors in reading the graphs.

2.1. Form and Purpose of Parametric Analysis

The parametric analysis of the probability density function mean before us is involved, and it might help to work through the principles in a simpler setting. Consider the normal distribution

$$\varphi(\chi; m, s) = \frac{1}{\sqrt{2\pi s^2}} e^{-\frac{(\chi-m)^2}{2s^2}}.$$

Throughout this paper, symbols in argument lists of functions will often have a semi-colon separating them. Symbols to the left of the semi-colon are variables, and those to the right are parameters. When working with model parameters, the first step is usually to identify them in some situation-specific way. For example, it can be shown that for φ, m is the mean of the probability distribution and s^2 is the variance. The next step in the analysis is to systematically vary a parameter while holding the others constant. In this setting, if we hold s constant and increase m, the familiar bell-shaped curve of the normal distribution shifts right. Decreasing m makes it shift left. Holding m constant and decreasing s makes the "bell" become tall and narrow. Increasing s causes the bell-shape to flatten out.

The situation in this paper is one step more complicated: the model parameters themselves depend on parameters. In our example, that would be the same as

$$m(;\alpha,\beta,\gamma) = f(\alpha,\beta,\gamma) \quad s(;\alpha,\beta,\gamma) = g(\alpha,\beta,\gamma)$$

We know that increasing m shifts the curve, but what causes m to increase? Now we must perform a parametric analysis on m in terms of the other model parameters. As part of this process, we might observe

$$\frac{\partial m}{\partial \alpha} > 0.$$

Therefore, we would conclude m increases as α increases. Hence, increasing α shifts the curve to the right. This type of analysis is typical of what follows.

2.2. Overview of the Eye-Tracking Model and Parametric Analysis

The method of development of our mathematical model occurs in several steps. The approach detailed is based on Bookstein's landmark model [21] adapted for eye tracking. First, we consider the geometry of the visualization, identifying important areas of interest. A fixation point $\mathbf{P}_i$ is selected from each AOI. A vector $\mathbf{z}_i$ points to the center of the AOI. We then decompose $\mathbf{P}_i$ as

$$\mathbf{P}_i = \mathbf{d}_i + \mathbf{z}_i. \tag{1}$$

Here, $\mathbf{z}_i$ is fixed and is determined by the geometry of the visualization, and $\mathbf{d}_i$ is a random vector marking the displacement about the center of the AOI (see Figures 3 and 4) . One point $\mathbf{P}_i$ is selected from each AOI, and these points are connected by line segments, forming a triangle. Since these points are randomly located, this forms a stochastic triangle (See Figure 3). Next, we find the probability distribution of a side length and take its mean. With that in hand, a parametric analysis of the expected visual measurement error is performed.

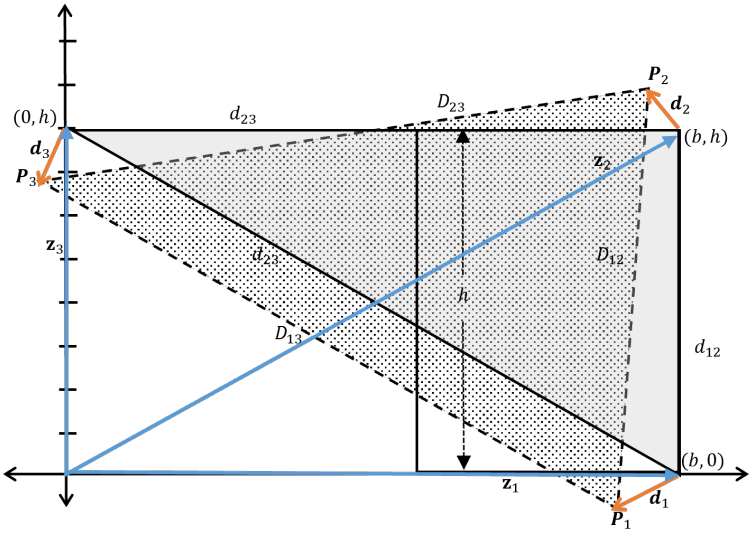


Figure 3. The fundamental stochastic triangle. $\mathbf{P}_i$ is a fixation, $\mathbf{z}_i$ (blue) is a fixed vector pointing to a key focal point, and $\mathbf{d}_i$ (orange) is the random displacement of the fixation about the focal point.

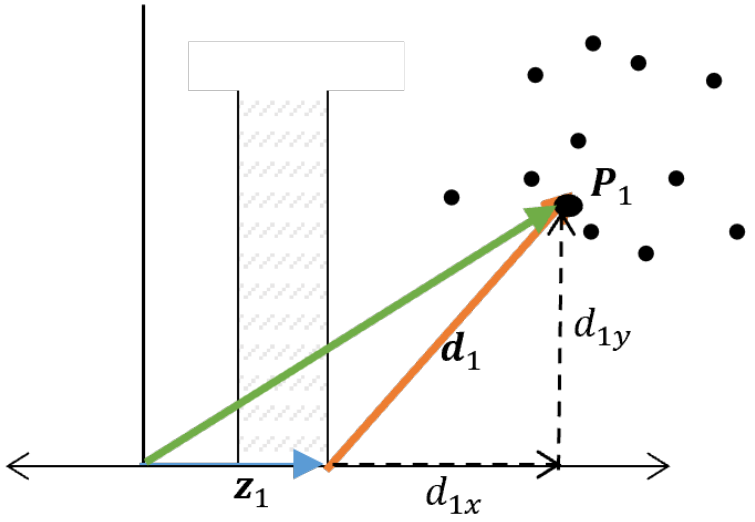


Figure 4. Labeling of the decomposition of the fixations. The dots are fixation points $\mathbf{P}_i$. The solid arrows represent the vectors in the decomposition $\mathbf{P}_i = \mathbf{d}_i + \mathbf{z}_i$. The dashed arrows are the horizontal and vertical components of $\mathbf{d}_i$.

2.3. Geometrical Considerations

Following the notation Stoyan and Stoyan [23] used in their section on the Bookstein model, we label the fixed reference points on the corners of the triangle as

$$\mathbf{z}_1 = \begin{bmatrix} b \\ 0 \end{bmatrix}, \quad \mathbf{z}_2 = \begin{bmatrix} b \\ h \end{bmatrix}, \quad \text{and} \quad \mathbf{z}_3 = \begin{bmatrix} 0 \\ h \end{bmatrix}. \tag{2}$$

Relative to the fixed points, the fixations $\mathbf{P}_i$ are $\mathbf{P}_i = \mathbf{d}_i + \mathbf{z}_i$, where

$$\mathbf{d}_i = \begin{bmatrix} d_{ix} \\ d_{iy} \end{bmatrix}. \tag{3}$$

The original side lengths are

$$\begin{aligned} d_{12} &= \|\mathbf{z}_2 - \mathbf{z}_1\| = \sqrt{(b-b)^2 + (h-0)^2} = h \\ d_{23} &= \|\mathbf{z}_3 - \mathbf{z}_2\| = \sqrt{(0-b)^2 + (h-h)^2} = b \\ d_{13} &= \|\mathbf{z}_3 - \mathbf{z}_1\| = \sqrt{(0-b)^2 + (h-0)^2} = \sqrt{b^2 + h^2}. \end{aligned}$$

Figure 3 shows the layout of the sides of the stochastic triangle. We begin with D_{12}:

$$\begin{aligned} D_{12} &= \|\mathbf{P}_2 - \mathbf{P}_1\| = \|(\mathbf{z}_2 + \mathbf{d}_2) - (\mathbf{z}_1 + \mathbf{d}_1)\| \\ &= \sqrt{((b + d_{2x}) - (b + d_{1x}))^2 + ((h + d_{2y}) - (0 + d_{1y}))^2} \\ &= \sqrt{((d_{2x} - d_{1x})^2 + (h + (d_{2y} - d_{1y}))^2}. \end{aligned}$$

Let $\eta = d_{2x} - d_{1x}$ and $\zeta = d_{2y} - d_{1y}$; we obtain

$$D_{12} = \sqrt{\eta^2 + (h + \zeta)^2}. \tag{4}$$

Similarly,

$$\begin{aligned} D_{23} &= \|\mathbf{P}_2 - \mathbf{P}_3\| \\ &= \sqrt{(b + \alpha)^2 + \beta^2} \end{aligned}$$

where $\alpha = d_{2x} - d_{3x}$ and $\beta = d_{2y} - d_{3y}$. And for $\gamma = d_{1x} - d_{3x}$ and $\omega = d_{1y} - d_{3y}$,

$$\begin{aligned} D_{13} &= \|\mathbf{P}_1 - \mathbf{P}_3\| \\ &= \sqrt{(b + \gamma)^2 + (h + \omega)^2}. \end{aligned}$$

2.4. General Case

The side length D_{12} is a random variable. The end objective is to find its probability density function and associated mean. This will involve the so-called *Gaussian distributions* [24]. To obtain these, we must be very precise about the model used for η and ζ. In his book [25], Miller has 45 different pdfs for Gaussian distribution processes based on subtle variations in the joint mean and correlation of these two random variables. We will explore this first under minimal assumptions and then for various specific cases.

2.4.1. Fixation Components

It is reasonable to assume that the fixations are balanced about the fixed points, such as $\mathbf{z}_1$. This makes, for $i = 1, 2, 3$,

$$\mathrm{E}(d_{ix}) = \mathrm{E}(d_{iy}) = 0. \tag{5}$$

Maintaining generality, for the variance,

$$\mathrm{Var}(d_{ix}) = \sigma_{ix}^2 \tag{6}$$

$$\mathrm{Var}(d_{iy}) = \sigma_{iy}^2 \tag{7}$$

for $i = 1, 2, 3$. It is traditional in landscape models to assume the horizontal and vertical components are uncorrelated; however, such is questionable in eye motion. As discussed in [18,19], horizontal and vertical movements behave differently. Horizontal movement of the eye is stronger and more accurate, whereas vertical movement is weaker. It behaves differently for up and down directions and often misses its mark by overshooting or undershooting. It frequently "fishtails" at the end to correct its location. Hence, in this model, it is allowed that a correlation exists, and the impact of the parameter is studied. To be specific, we name

$$\rho_i = \mathrm{corr}(d_{ix}, d_{iy}) \quad \text{for} \quad i = 1, 2, 3. \tag{8}$$

It now assumed that the fixations are normally distributed about the fixed points $\mathbf{z}_i$, resulting in

$$\begin{bmatrix} d_{ix} \\ d_{iy} \end{bmatrix} = N_2\left(\begin{bmatrix} 0 \\ 0 \end{bmatrix}, \begin{bmatrix} \sigma_{ix}^2 & \rho_i \sigma_{ix} \sigma_{iy} \\ \rho_i \sigma_{ix} \sigma_{iy} & \sigma_{iy}^2 \end{bmatrix} \right). \tag{9}$$

The variance matrix must be invertible, leading to the requirement

$$\det \begin{bmatrix} \sigma_{ix}^2 & \rho_i \sigma_{ix} \sigma_{iy} \\ \rho_i \sigma_{ix} \sigma_{iy} & \sigma_{iy}^2 \end{bmatrix} = \sigma_{ix}^2 \sigma_{iy}^2 (1 - \rho_i^2) > 0 \tag{10}$$

for $i = 1, 2, 3$, which is satisfied if the correlation is $-1 < \rho_i < 1$.

2.4.2. Side Lengths

Recalling Equation (4), in order to find the probability distribution of D_{12}, the distributions of η and ζ must be calculated. First,

$$\mathrm{E}(\eta) = \mathrm{E}(d_{2x} - d_{1x}) = 0.$$

Similarly,

$$\mathrm{E}(\zeta) = \mathrm{E}(d_{2y} - d_{1y}) = 0.$$

For the variance,

$$\begin{aligned} \mathrm{Var}(\eta) &= \mathrm{Var}(d_{2x} - d_{1x}) \\ &= \mathrm{Var}(d_{2x}) + \mathrm{Var}(d_{1x}) - 2\,\mathrm{Cov}(d_{2x}, d_{1x}) \\ &= \mathrm{Var}(d_{2x}) + \mathrm{Var}(d_{1x}) - 2\,\mathrm{corr}(d_{2x}, d_{1x}) \sqrt{\mathrm{Var}(d_{2x})\,\mathrm{Var}(d_{1x})} \\ &= \sigma_{2x}^2 + \sigma_{1x}^2 - 2\,\mathrm{corr}(d_{2x}, d_{1x}) \sigma_{2x} \sigma_{1x}. \end{aligned}$$

The term $\mathrm{corr}(d_{2x}, d_{1x})$ requires discussion. The first correlation term encountered, ρ_i, involves the horizontal and vertical components of the fixation about the same fixed point. This term is the correlation between the horizontal components of adjacent fixed points. On the one hand, it could be argued that the fixations in the AOIs about different fixed points are independent, which was considered in [26]. In this case, $\mathrm{corr}(d_{2x}, d_{1x}) = 0$. On the other hand, considering the scanpath of the eye about the triangle, the model views the eye moving rapidly from one AOI to another. It seems possible that the horizontal offsets between the fixed points would influence each other, leading to a nonzero correlation. In the spirit of generality, then the correlation is maintained in the model, at least in this case, so that

$$\rho_{12x} = \mathrm{corr}(d_{2x}, d_{1x}) \tag{11}$$

and

$$\mathrm{Var}(\eta) = \sigma_{2x}^2 + \sigma_{1x}^2 - 2\rho_{12x}\sigma_{2x}\sigma_{1x}. \tag{12}$$

Denoting

$$\rho_{12y} = \mathrm{corr}(d_{2y}, d_{1y}) \tag{13}$$

similar calculations show

$$\mathrm{Var}(\zeta) = \sigma_{2y}^2 + \sigma_{1y}^2 - 2\rho_{12y}\sigma_{2y}\sigma_{1y}. \tag{14}$$

The covariance presents different issues. It is

$$\begin{aligned}\mathrm{Cov}(\eta,\zeta) &= \mathrm{E}(\eta\zeta) - \mathrm{E}(\eta)\,\mathrm{E}(\zeta)\\ &= \mathrm{E}(\eta\zeta) = \mathrm{E}((d_{2x} - d_{1x})(d_{2y} - d_{1y}))\\ &= \mathrm{E}(d_{2x}d_{2y}) - \mathrm{E}(d_{2x}d_{1y}) - \mathrm{E}(d_{1x}d_{2y}) + \mathrm{E}(d_{1x}d_{1y}).\end{aligned}$$

The first and last terms have been encountered. They are

$$\begin{aligned}\mathrm{E}(d_{1x}d_{1y}) &= \rho_1\\ \mathrm{E}(d_{2x}d_{2y}) &= \rho_2.\end{aligned}$$

The remaining terms again require modeling consideration. Again, the correlation around adjacent fixed points is encountered. This time it is the horizontal component at one point and the vertical component at the other. The previous discussion remains relevant, and the general case is considered. Here, we introduce the correlations

$$\rho_{1y2x} = \mathrm{corr}(d_{1y}, d_{2x}) \tag{15}$$

$$\rho_{1x2y} = \mathrm{corr}(d_{1x}, d_{2y}) \tag{16}$$

allowing one to write the covariance as

$$\mathrm{Cov}(\eta,\zeta) = \rho_1\sigma_{1x}\sigma_{1y} + \rho_2\sigma_{2x}\sigma_{2y} - \rho_{1y2x}\sigma_{1y}\sigma_{2x} - \rho_{1x2y}\sigma_{1x}\sigma_{2y}. \tag{17}$$

2.5. Special Cases

With the general case stated, several useful specializations can be enumerated. As will be elaborated, the problem in its full generality is, as of now, intractable. The first simplifying assumption to be made is that all the correlations have the same value. Namely,

$$\rho = \rho_1 = \rho_2 = \rho_{12x} = \rho_{12y} = \rho_{1y2x} = \rho_{1x2y}. \tag{18}$$

Under this assumption, the general case becomes

$$\hat{\mathbf{\Lambda}} = \mathrm{Cov}(\eta,\zeta) = \begin{bmatrix}\hat{\sigma}_1^2 & \hat{\sigma}_{12}\\ \hat{\sigma}_{12} & \hat{\sigma}_2^2\end{bmatrix} \tag{19}$$

where

$$\hat{\sigma}_1^2 = \sigma_{1x}^2 + \sigma_{2x}^2 - 2\rho\sigma_{1x}\sigma_{2x} \tag{20}$$

$$\hat{\sigma}_2^2 = \sigma_{1y}^2 + \sigma_{2y}^2 - 2\rho\sigma_{1y}\sigma_{2y} \tag{21}$$

$$\hat{\sigma}_{12} = \rho(\sigma_{1x}\sigma_{1y} + \sigma_{2x}\sigma_{2y} - \sigma_{1y}\sigma_{2x} - \sigma_{1x}\sigma_{2y}). \tag{22}$$

In order to proceed with further analysis, simplifications of this system are required. The most progress has been made on positive definite diagonal variance matrices. This means one should examine cases in which η and ζ are not correlated. Note, in situations in which $\mathrm{corr}(\eta,\zeta) = 0$, the eye motion associated with the fixations can still be correlated. That is, $\rho \neq 0$.

A further common restriction on the problem is

$$\mathbf{\Lambda} = \begin{bmatrix} \psi_0^2 & 0 \\ 0 & \psi_0^2 \end{bmatrix} = \psi_0^2 \mathbf{I} \tag{23}$$

where $\mathbf{I}$ is the identity matrix. That is, $\mathbf{\Lambda}$ is a diagonal matrix with the same positive number as its diagonal elements. (At the moment, ψ_0^2 is just a label and has no interpretation in terms of model parameters. In the following, specific examples will be given.) Equation (23) being a common assumption might be surprisingly strong, but Miller says in [25] that determining the probability density function for an arbitrary positive definite *diagonal* covariance matrix proves to be "extremely difficult".

Shortly, we will work through several cases for $\mathbf{\Lambda}$ by populating it with model parameters. In each case, restrictions are put into place to simplify Equation (19). We will see that various restrictions applied in combination can produce a diagonal matrix with identical elements on the diagonal, like Equation (23), as well as unequal elements on the diagonal. Furthermore, we will demonstrate that we can recover the same model as Stoyan and Stoyan's [23] by using restrictions similar to theirs.

Progress has been made on the 2×2 correlated case, but an interesting snag arises. To explain this, material from the next section must be briefly considered. In that section, a normalization process is performed. Namely,

$$X_1 = \frac{\eta}{\hat{\sigma}_1} \qquad X_2 = \frac{\zeta + h}{\hat{\sigma}_2}. \tag{24}$$

The problem is that $\mathrm{E}(X_1) = 0$ and $\mathrm{E}(X_2) = h/\hat{\sigma}_2$. Finding the joint pdf for two variables having different means in conjunction with a non-diagonal covariance matrix is still an open question. The author has some results on this and will submit them in future publications.

Now, various cases will be considered that remove the correlation between η and ζ, which allows nontrivial relations for the mean.

2.5.1. Case A: Diagonal Covariance Matrix with the Same Diagonal Elements

This is the case typically considered in the literature on the Bookstein model [21]. In this situation,

$$\sigma = \sigma_{1x} = \sigma_{2x} = \sigma_{1y} = \sigma_{2y}. \tag{25}$$

This means

$$\begin{aligned} \hat{\sigma}_1^2 &= \sigma^2 + \sigma^2 - 2\rho\sigma\sigma = 2\sigma^2(1-\rho) \\ \hat{\sigma}_2^2 &= \sigma^2 + \sigma^2 - 2\rho\sigma\sigma = 2\sigma^2(1-\rho) \\ \hat{\sigma}_{12} &= \rho(\sigma\sigma + \sigma\sigma - \sigma\sigma - \sigma\sigma) = 0. \end{aligned}$$

Writing this in matrix notation,

$$\mathbf{\Lambda}_A = \begin{bmatrix} 2\sigma^2(1-\rho) & 0 \\ 0 & 2\sigma^2(1-\rho) \end{bmatrix} = \psi_A^2 \mathbf{I}$$

where $\psi_A^2 = 2\sigma^2(1-\rho)$.

A few observations are in order. The correlation between the various fixations satisfies $-1 < \rho < 1$. This means $\psi_A^2 > 0$. However, as ρ nears 1 from below, the variance becomes nearly singular. The determinant is $\det(\mathbf{\Lambda}_A) = 4\sigma^4(1-\rho)^2 > 0$ as long as $\rho < 1$. The significance of ρ is important. No other investigations have included a correlation between the horizontal and vertical components. It will be seen that there is a difference in behavior for positive and negative correlation.

2.5.2. Case B: Diagonal Covariance Matrix with Different Diagonal Elements

We present three situations in which this can happen.

Case B1: Set $\sigma_y = \sigma_{1y} = \sigma_{2y}$.
In this case,

$$\begin{aligned}\hat{\sigma}_1^2 &= \sigma_{1x}^2 + \sigma_{2x}^2 - 2\rho\sigma_{1x}\sigma_{2x}\\ \hat{\sigma}_2^2 &= \sigma_y^2 + \sigma_y^2 - 2\rho\sigma_y\sigma_y = 2\sigma_y^2(1-\rho)\\ \hat{\sigma}_{12} &= \rho(\sigma_{1x}\sigma_y + \sigma_{2x}\sigma_y - \sigma_y\sigma_{2x} - \sigma_{1x}\sigma_y) = 0\end{aligned}$$

or in matrix notation,

$$\mathbf{\Lambda}_{B1} = \begin{bmatrix}\sigma_{1x}^2 + \sigma_{2x}^2 - 2\rho\sigma_{1x}\sigma_{2x} & 0\\ 0 & 2\sigma_y^2(1-\rho)\end{bmatrix}.$$

Case B2: Set $\sigma_x = \sigma_{1x} = \sigma_{2x}$.
With calculations analogous to those above, the covariance matrix is found to be

$$\mathbf{\Lambda}_{B2} = \begin{bmatrix}2\sigma_x^2(1-\rho) & 0\\ 0 & \sigma_{1y}^2 + \sigma_{2y}^2 - 2\rho\sigma_{1y}\sigma_{2y}\end{bmatrix}.$$

Case B3: Set $\sigma_x = \sigma_{1x} = \sigma_{2x} \quad \sigma_y = \sigma_{1y} = \sigma_{2y}$.
This case yields the two previous to obtain

$$\mathbf{\Lambda}_{B3} = \begin{bmatrix}2\sigma_x^2(1-\rho) & 0\\ 0 & 2\sigma_y^2(1-\rho)\end{bmatrix}.$$

2.5.3. Case C: Bookstein's Model Assumptions

In Stoyan and Stoyan's book [23], they report the following assumptions with regard to the Bookstein model:

$$\sigma_1 = \sigma_{1x} = \sigma_{1y} \qquad \sigma_2 = \sigma_{2x} = \sigma_{2y}.$$

Under these assumptions, the model of this paper becomes

$$\begin{aligned}\hat{\sigma}_1^2 &= \sigma_1^2 + \sigma_2^2 - 2\rho\sigma_1\sigma_2\\ \hat{\sigma}_2^2 &= \sigma_1^2 + \sigma_2^2 - 2\rho\sigma_1\sigma_2\\ \hat{\sigma}_{12} &= \rho(\sigma_1^2 + \sigma_2^2 - 2\sigma_1\sigma_2).\end{aligned}$$

Hence, the covariance matrix is

$$\mathbf{\Lambda}_C = \begin{bmatrix}\sigma_1^2 + \sigma_2^2 - 2\rho\sigma_1\sigma_2 & \rho(\sigma_1^2 + \sigma_2^2 - 2\sigma_1\sigma_2)\\ \rho(\sigma_1^2 + \sigma_2^2 - 2\sigma_1\sigma_2) & \sigma_1^2 + \sigma_2^2 - 2\rho\sigma_1\sigma_2.\end{bmatrix}.$$

It is seen then that η and ζ are correlated under these assumptions in this model, though the model does have the same values on the diagonal. Of course, in their approach, there was no correlation between the horizontal and vertical components. Setting $\rho = 0$, their model is recovered.

2.6. Side Length Probability Density Function

In this section, the focus is on the determination of the probability density function of the height of bar D_{12} (Equation (4)). As previously mentioned, the next step is to normalize the variables using the transform given in Equation (24). This highlights the need for a simplifying assumption. The elements of the diagonal of the covariance matrix are seen in

the denominator. In Case A, these values are equal. So, as has been done in the previous investigations of the Bookstein model, Case A is assumed. Namely,

$$\psi_A = \hat{\sigma}_1 = \hat{\sigma}_2 = \sqrt{2\sigma^2(1-\rho)}.$$

Hence,

$$X_1 = \frac{\eta}{\psi_A} \qquad X_2 = \frac{\zeta + h}{\psi_A}.$$

This allows one to write

$$\begin{aligned} D_{12} &= \sqrt{\psi_A^2\left(\left(\frac{\eta}{\psi_A}\right)^2 + \left(\frac{\zeta+h}{\psi_A}\right)^2\right)} \\ &= \sqrt{\psi_A^2(X_1^2 + X_2^2)} \end{aligned}$$

or

$$\frac{D_{12}}{\psi_A} = \sqrt{X_1^2 + X_2^2}.$$

It follows that

$$\mathrm{E}(X_1) = 0 \qquad\qquad \mathrm{E}(X_2) = h/\psi_A$$

which is the aforementioned situation in which the means of the variables are different, prompting the need for a simple covariance structure.

The variable $y = D_{12}/\psi_a$ has the generalized Rayleigh distribution, which is also called the noncentral chi distribution (not to be confused with the chi-squared distribution) or Rice distribution [27,28]. The noncentrality parameter is

$$y_0^2 = \sum_{j=1}^{2} \mathrm{E}(X_j)^2 = h^2/\psi_A^2.$$

According to Park [29], the probability density function is

$$\begin{aligned} g(y; y_0) &= y \exp[(y^2 + y_0^2)/2] I_0(y y_0) H(y) \\ g(y; h, \psi_A) &= y \exp[(y^2 + h^2/\psi_A^2)/2] I_0(y(h/\psi_A)) H(y). \end{aligned}$$

In this expression, I_0 is a modified Bessel function of the first kind of order zero, and $H(y)$ is the Heavyside function.

3. Results

With the model formulated and the basic probability density function determined, it is appropriate to begin the analysis of key features of interest. Once the mean of D_{12} is given, a parametric analysis is performed. This will offer insight into possible sources of the expected visual measurement error as well as confirm basic characteristics of favorable design features.

3.1. The Mean and Useful Properties

By definition,

$$\mathrm{E}(D_{12}/\psi_A) = \int_0^\infty y g(y) dy. \tag{26}$$

Park determined this mean [29]. Multiplying by ψ_A, he found

$$\mu = \mathrm{E}(D_{12}) = \psi_A \sqrt{2} \exp\left(-\frac{h^2}{2\psi_A^2}\right) \frac{\Gamma(3/2)}{\Gamma(1)} \, {}_1\mathrm{F}_1\left(\frac{3}{2}; 1; \frac{h^2}{2\psi_A^2}\right) \tag{27}$$

where ${}_1\mathrm{F}_1(a; b; x)$ is the confluent hypergeometric function. It is also denoted as $\mathrm{M}(a, b, x)$ by several important authors. It is labeled this way to be consistent with generalized hypergeometric functions.

There will be need for the power series expansion of ${}_1\mathrm{F}_1(a; b; x)$. For $z \in \mathbb{C}$,

$${}_1\mathrm{F}_1(a; b; z) = \sum_{s=0}^{\infty} \frac{(a)_s}{(b)_s s!} z^s = 1 + \frac{a}{b} z + \frac{a(a+1)}{b(b+1)2!} z^2 + \ldots \quad (b \neq 0, -1, -2, -3, \ldots) \tag{28}$$

where $(a)_s$ is the Pochhammer symbol with the properties

$$\begin{aligned} (a)_0 &= 1 \\ (a)_n &= a(a+1)(a+2)\ldots(a+n-1) = \frac{\Gamma(a+n)}{\Gamma(a)}. \end{aligned}$$

The Gamma function is used repeatedly, so a few useful properties are given for the convenience of the reader:

$$\begin{aligned} \Gamma(n) &= (n-1)! & & n = 1, 2, 3, \ldots \\ \Gamma(z+1) &= z\Gamma(z) & & z \in \mathbb{C} \\ \Gamma(1/2) &= \sqrt{\pi} & & \\ \Gamma(3/2) &= \sqrt{\pi}/2. & & \end{aligned}$$

As the confluent hypergeometric function is less common and yet critical to the analysis, several of its basic properties are given. Then, a simple lemma encapsulating useful attributes is proven. Many features of this function are available in the *NIST Handbook of Mathematical Functions* [30]. (The numbers below, such as (13.2.39), locate the given equation in the sizable NIST reference [30] and are provided for ease of reference for those who wish to explore other properties of this remarkable function).

1. The power series in Equation (28) for ${}_1\mathrm{F}_1(a; b; z)$ is entire in z and a and meromorphic in b for $b \neq 0, -1, -2, \ldots$;
2. Kummer's theorem states

$${}_1\mathrm{F}_1(a; b; z) = e^z \, {}_1\mathrm{F}_1(b-a; b; -z) \quad (13.2.39); \tag{29}$$

3. Recurrence relationship

$$b \, {}_1\mathrm{F}_1(a; b; z) - b \, {}_1\mathrm{F}_1(a-1; b; z) - z \, {}_1\mathrm{F}_1(a; b+1; z) = 0 \quad (13.3.4); \tag{30}$$

4. Derivative formulae

$$\frac{d}{dz} \, {}_1\mathrm{F}_1(a; b; z) = \frac{a}{b} \, {}_1\mathrm{F}_1(a+1; b+1; z) \quad (13.3.15) \tag{31}$$

and

$$\frac{d}{dz}(e^{-z} \, {}_1\mathrm{F}_1(a; b; z)) = (-1)^1 \frac{(b-a)_1}{(b)_1} e^{-z} \, {}_1\mathrm{F}_1(a; b+1; z) \quad (13.3.20). \tag{32}$$

Now, we provide a lemma concerning ${}_1\mathrm{F}_1(a; b; x)$ that is used extensively.

Lemma 1. *For $a, b \in \mathbb{R}$ such that $a, b > 0$ and $x \in \mathbb{R}$,*

1. ${}_1\mathrm{F}_1(a; b; x) \in \mathbb{R}$;

2. ${}_1\mathrm{F}_1(a;b;x) > 0$;
3. ${}_1\mathrm{F}_1(a;b;x)$ *is strictly increasing in* x;
4. *For* $x > 0$, ${}_1\mathrm{F}_1(a;b;x) > 1$.

Proof. (1) This follows immediately from the power series expansion in Equation (28) and that a, b, and x are real numbers and b is positive. Since the real numbers are closed under arithmetic operations ($b > 0$ excludes division by zero) and are complete, the power series converges to a real number.

(2) It is given in [30] that for $a, b > 0$, ${}_1\mathrm{F}_1(a;b;x)$ has no real zeros. Again, from the power series, it is seen that ${}_1\mathrm{F}_1(a;b;0) = 1$. Hence, ${}_1\mathrm{F}_1(a;b;x)$ must remain positive for all real values of x.

(3) By Equation (31),

$$\frac{d}{dx}\,{}_1\mathrm{F}_1(a;b;x) = \frac{a}{b}\,{}_1\mathrm{F}_1(a+1,b+1,x)$$

and since $a+1 > a > 0$ and $b+1 > b > 0$, part 2 that was just proven can be applied using $a+1$ and $b+1$ to conclude

$$\frac{d}{dx}\,{}_1\mathrm{F}_1(a;b;x) = \frac{a}{b}\,{}_1\mathrm{F}_1(a+1,b+1,x) > 0.$$

Hence, ${}_1\mathrm{F}_1(a;b;x)$ is strictly increasing in x.

(4) For $0 < x$, $1 = {}_1\mathrm{F}_1(a;b;0) < {}_1\mathrm{F}_1(a;b;x)$ since it is strictly increasing in x. Hence, the result follows. □

3.2. Parametric Behavior of the Mean

Many parameters have been introduced into this model: so many that their number was reduced to produce a model that was tractable with currently available mathematical machinery. The set that remains includes the height of the bar (h), a correlation of the fixations (ρ), a variance of the fixations (ψ), and the noncentrality parameter of the chi distribution of the side length ($\lambda = h/\psi$). (The subscript A is dropped from ψ for simplicity, as it is understood.) Closely related to λ is a scale ($\tau = \sigma/h$). In working with this model, σ appears almost exclusively in ratio with h, allowing relabeling with τ. It has been found in simulations and real data analyses that τ is a critical indicator of the success of the method under consideration. Therefore, the analysis to follow will focus on h, λ, τ, and ρ. If needed, we can always write $\sigma = h\tau$. No claim is being made that these form a minimal set of parameters.

3.2.1. Parametric Representation of the Mean

Using $\Gamma(3/2) = \sqrt{\pi}/2$ and $\Gamma(1) = 1$ along with the following relationships between parameters

$$\psi = \sqrt{2}\sigma\sqrt{1-\rho} \tag{33}$$

$$= \sqrt{2}h\tau\sqrt{1-\rho} \tag{34}$$

$$\lambda = \frac{h}{\psi} \tag{35}$$

the mean in Equation (27) can be expressed in terms of the various parameters as

$$\mu(\sigma;h,\rho) = h\left(\sqrt{\pi}\sigma\exp\left(-\frac{h^2}{2\sigma^2(1-\rho)}\right){}_1\mathrm{F}_1\left(3/2;1;\frac{h^2}{2\sigma^2(1-\rho)}\right)\right) \tag{36}$$

$$\mu(\rho;h,\tau) = h\left(\sqrt{\pi}\tau\sqrt{1-\rho}\exp\left(-\frac{1}{4\tau^2(1-\rho)}\right){}_1\mathrm{F}_1\left(3/2;1;\frac{1}{4\tau^2(1-\rho)}\right)\right) \tag{37}$$

$$\mu(\tau;h,\rho) = h\left(\sqrt{\pi}\tau\sqrt{1-\rho}\exp\left(-\frac{1}{4\tau^2(1-\rho)}\right){}_1\mathrm{F}_1\left(3/2;1;\frac{1}{4\tau^2(1-\rho)}\right)\right) \tag{38}$$

$$\mu(\lambda;h) = h\left(\sqrt{\frac{\pi}{2}}\frac{\exp\left(-\lambda^2/2\right)}{\lambda}{}_1\mathrm{F}_1\left(3/2;1;\lambda^2/2\right)\right) \tag{39}$$

3.2.2. General Framework for Parametric Analysis

For purposes of discussion, let θ be one of the parameters in the model. The analysis proceeds by first finding the derivative of the mean (μ) with respect to θ. This is used in conjunction with Lemma 1 to determine if the mean is monotone in θ. Next, the asymptotic properties of both μ and $d\mu/d\theta$ are examined.

These objectives will be facilitated by the next two theorems. Theorem 1 provides half of a chain rule argument needed to determine the derivative of μ with respect to θ. Unfortunately, the derivatives cannot follow as simple corollaries because their nonlinear, coupled nature makes each case different, and they must be handled separately. With that said, Theorem 2 supplies an asymptotic analysis that can be easily exploited to obtain the large (or small) θ behavior of μ.

3.2.3. An Intermediate Form for Analysis

It is convenient for purposes of analysis to derive an intermediate expression for the mean in terms of the ratio of certain parameters. Namely,

$$u(\psi) = \frac{h^2}{2\psi^2} = \frac{h^2}{4h^2\tau^2(1-p)}. \tag{40}$$

Equation (27) becomes

$$\mu = \sqrt{\frac{\pi}{2}}\psi\exp(-u(\psi)){}_1\mathrm{F}_1(3/2;1;u(\psi)). \tag{41}$$

Note that ψ can be written in terms of u as

$$\psi = \frac{h}{\sqrt{2}\sqrt{u}} \tag{42}$$

and μ becomes a function of u as

$$\mu(u;h) = h\frac{\sqrt{\pi}}{2}\frac{\mathrm{e}^{-u}}{\sqrt{u}}{}_1\mathrm{F}_1(3/2;1;u). \equiv h\Phi(u) \tag{43}$$

for $u > 0$. In much of the analysis to follow, the function $\Phi(u)$ plays a critical role. Expressions in one set of parameters will be transformed into $\Phi(u)$, and its properties will be exploited. Hence, two fundamental results about it are given.

Theorem 1. *The function*

$$\Phi(u) = \frac{\sqrt{\pi}}{2}\frac{\mathrm{e}^{-u}}{\sqrt{u}}{}_1\mathrm{F}_1(3/2;1;u) \tag{44}$$

is decreasing for positive values of u.

Proof. Taking the derivative of both sides of Equation (44) with respect to u gives

$$\frac{2}{\sqrt{\pi}}\frac{d\Phi}{du}(u) = \left(\frac{d}{du}\frac{1}{\sqrt{u}}\right)\mathrm{e}^{-u}\,{}_1\mathrm{F}_1(3/2;1;u) \quad + \\ \frac{1}{\sqrt{u}}\frac{d}{du}(\mathrm{e}^{-u}\,{}_1\mathrm{F}_1(3/2;1;u)). \tag{45}$$

Using Equation (32) gives

$$\begin{aligned}\frac{d}{du}(\mathrm{e}^{-u}\,{}_1\mathrm{F}_1(3/2;1;u)) &= (-1)\frac{(1-3/2)_1}{(1)_1}\,\mathrm{e}^{-u}\,{}_1\mathrm{F}_1(3/2,1+1,u)\\ &= (-1)(-1/2)\,\mathrm{e}^{-u}\,{}_1\mathrm{F}_1(3/2;2;u)\\ &= (1/2)\,\mathrm{e}^{-u}\,{}_1\mathrm{F}_1(3/2;2;u).\end{aligned}$$

Combining these into Equation (45) gives

$$\frac{2}{\sqrt{\pi}}\frac{d\Phi(u)}{du} = -\frac{1}{2}u^{-3/2}\,\mathrm{e}^{-u}\,{}_1\mathrm{F}_1(3/2;1;u) + \frac{1}{2}u^{-1/2}\,\mathrm{e}^{-u}\,{}_1\mathrm{F}_1(3/2;2;u) \tag{46}$$

$$= \frac{\mathrm{e}^{-u}}{2u^{3/2}}[-\,{}_1\mathrm{F}_1(3/2;1;u) + u\,{}_1\mathrm{F}_1(3/2;2;u)]. \tag{47}$$

Now, the recurrence in Equation (30) is applied with $a = 3/2$ and $b = 1$:

$${}_1\mathrm{F}_1(3/2;1;u) - {}_1\mathrm{F}_1(1/2,1/u) - u\,{}_1\mathrm{F}_1(3/2;2;u) = 0$$

or

$$-\,{}_1\mathrm{F}_1(3/2;1;u) + u\,{}_1\mathrm{F}_1(3/2;2;u) = -\,{}_1\mathrm{F}_1(1/2;1;u). \tag{48}$$

Substituting Equation (48) into Equation (47) yields for positive values u:

$$\frac{d\Phi}{du} = -\frac{\sqrt{\pi}}{4}\frac{\mathrm{e}^{-u}}{u^{3/2}}\,{}_1\mathrm{F}_1(1/2;1;u) < 0. \tag{49}$$

by Lemma 1. It follows that $\Phi(u)$ is a decreasing function of u. □

From this, we have immediately

$$\frac{d\mu}{du} = h\frac{d\Phi}{du} = -h\frac{\sqrt{\pi}}{4}\frac{\mathrm{e}^{-u}}{u^{3/2}}\,{}_1\mathrm{F}_1(1/2;1;u). \tag{50}$$

Now, a general theorem is proven for the variable u, binding together the key parameters in the way they naturally appear for the expected value of the length of a side of the triangle.

Theorem 2. *For $\Phi(u)$, defined in Equation (44),*

$$\Phi(u) \sim 1 \tag{51}$$

as $u \to \infty$.

Proof. In [30], (13.2.23) and (13.2.4) can be combined to give

$${}_1\mathrm{F}_1(a;b;z) \sim \frac{\Gamma(b)}{\Gamma(a)}\,\mathrm{e}^{z}\,z^{a-b} \quad z \to \infty, |phz| \le \frac{\pi}{2} - \delta \tag{52}$$

when δ is an arbitrarily small positive number. (This does not hold for the polynomial cases $a = 0, -1, -2, \ldots$.) In particular,

$$ {}_1\mathrm{F}_1(3/2;1;u) \sim \frac{\Gamma(1)}{\Gamma(3/2)}\, \mathrm{e}^u\, u^{3/2-1}. $$

Since $\Gamma(1) = 1$ and $\Gamma(3/2) = \sqrt{\pi}/2$, this yields

$$ {}_1\mathrm{F}_1(3/2;1;u) \sim \frac{2}{\sqrt{\pi}}\, \mathrm{e}^u\, \sqrt{u}. \tag{53} $$

Using Equation (53) in Equation (44), one obtains

$$ \Phi(u) \sim 1 \frac{\sqrt{\pi}}{2} \frac{\mathrm{e}^{-u}}{\sqrt{u}} \frac{2}{\sqrt{\pi}}\, \mathrm{e}^u\, \sqrt{u} = 1 \quad u \to \infty. \tag{54} $$

□

Using this, we have from Equation (43) and Theorem 2 that

$$ \mu(u;h) \sim h \quad u \to \infty \tag{55} $$

3.2.4. Analysis of the Correlation Parameter

In order to do a parametric analysis of $\mu(\rho;h,\tau)$, it is sufficient to use material in the proof of Theorem 1 and do a chain rule argument. The following corollary summarizes the results.

Corollary 1. *$\mu(\rho;h,\tau)$, given in Equation (37), is a decreasing function of ρ over the interval $(-1,1)$.*

Proof. The proof proceeds by transforming $\mu(\rho;h,\tau)$ into the intermediate form using

$$ u = \frac{h^2}{2\psi^2} \qquad\qquad \psi = \sqrt{2}h\tau\sqrt{1-\rho}. $$

then taking the derivative with respect to ρ and showing it is negative. We rewrite Equation (37) as

$$ \mu(\rho;h,\tau) = \left(\sqrt{\frac{\pi}{2}} \sqrt{2}h\tau\sqrt{1-\rho} \exp\left(-\frac{h^2}{4h^2\tau^2(1-\rho)} \right) {}_1\mathrm{F}_1\left(3/2;1; \frac{h^2}{4h^2\tau^2(1-\rho)} \right) \right). $$

Noting

$$ \sqrt{2}h\tau\sqrt{1-\rho} = \frac{h}{\sqrt{2u}} \tag{56} $$

and substituting, we obtain

$$ \mu(u;h) = h \frac{\sqrt{\pi}}{2} \frac{\mathrm{e}^{-u}}{\sqrt{u}}\, {}_1\mathrm{F}_1(3/2;1;u). \tag{57} $$

By the chain rule,

$$ \frac{d\mu}{d\rho} = \frac{d\mu}{du} \frac{du}{d\psi} \frac{d\psi}{d\rho}. \tag{58} $$

We have

$$ \frac{du}{d\psi} = -\frac{2}{\psi} u \tag{59} $$

and

$$\frac{d\psi}{d\rho} = -\frac{h\tau}{\sqrt{2}}\frac{1}{\sqrt{1-\rho}}. \tag{60}$$

Using Equation (59), Equation (60), and Equation (50) in Equation (58) gives

$$\frac{d\mu}{d\rho} = -h\frac{\sqrt{\pi}}{4}\frac{e^{-u}}{u^{3/2}}\,{}_1F_1(1/2;1;u)\left(-\frac{2}{\psi}u\right)\left(-\frac{h\tau}{\sqrt{2}}\frac{1}{\sqrt{1-\rho}}\right). \tag{61}$$

After canceling cross-terms, we apply

$$\frac{1}{\sqrt{u}} = \frac{\sqrt{2}\psi}{h}$$

and

$$u = \frac{h^2}{2\psi^2} = \frac{1}{4\tau^2(1-\rho)}$$

to return to the original variables, obtaining

$$\frac{d\mu}{d\rho}(\rho;h,\tau) = -h\frac{\sqrt{\pi}}{2}(\tau)\frac{e^{-\frac{1}{4\tau^2(1-\rho)}}}{\sqrt{1-\rho}}\,{}_1F_1\left(1/2;1;\frac{1}{4\tau^2(1-\rho)}\right). \tag{62}$$

From this, it is seen that $d\mu/d\rho < 0$ by part 2 of Lemma 1 over the interval $-1 < \rho < 1$. Therefore, $\mu(\rho;h,\tau)$ is decreasing as ρ approaches 1 from below. □

We now know that the expected length of a side of the triangle actually decreases as the fixation points become more strongly correlated in a positive sense. (We are discussing that the particular side connecting two points labeled one and two impacts the model only through the value of the noncentrality parameter. Ultimately, the value we labeled as h^2 could become b^2 or $h^2 + b^2$. We have chosen the stochastic edge D_{12} because of its association with the eye attempting to measure the height of the bar.)

Corollary 2. *For $\mu(\rho;h,\tau)$, given in Equation (37),*

$$\mu(\rho;h,\tau) \sim h. \tag{63}$$

as $\rho \to 1^-$.

Proof. It was shown in the proof of Corollary 1 that $\mu(\rho;h,\tau)$ can be transformed into the intermediate form using

$$u = \frac{h^2}{2\psi^2} \qquad\qquad \psi = \sqrt{2}h\tau\sqrt{1-\rho},$$

which can be written as

$$\mu(u;h) = h\Phi(u).$$

It is easily seen that $u \to \infty$ as $\rho \to 1^-$ and vice versa as τ is fixed. In this case, Theorem 2 is applied to show us $\Phi(u) \sim 1$ and, therefore, $\mu(\rho;h,\tau) \sim h$. □

If it were true that $d\mu/d\rho = 0$ everywhere, then the correlation introduced in the model has no influence on the mean length of the sides of the stochastic triangles for estimating the bar height visually. That is not that case, however, as Corollary 1 shows the derivative is nonzero everywhere over $(-1,1)$. In order to understand the nature of this, the following theorem was proven. Discussion will follow to explain it from an eye-tracking perspective.

Theorem 3. *For* $\frac{d\mu}{d\rho}(\rho; h, \tau)$*, given in Equation (62),*

$$\frac{d\mu}{d\rho} \sim -h\tau^2. \tag{64}$$

as $\rho \to 1^-$

Proof. Using (10.6.9) from the NIST handbook [30], one can relate the confluent hypergeometric function to the modified Bessel function of the first kind of order zero. We have

$${}_1\mathrm{F}_1\left(1/2; 1; 2\frac{1}{8\tau^2(1-\rho)}\right) = \mathrm{e}^{\frac{1}{8\tau^2(1-\rho)}}\,\mathrm{I}_0\left(\frac{1}{8\tau^2(1-\rho)}\right). \tag{65}$$

Let

$$w = \frac{1}{8\tau^2(1-\rho)}$$

so that

$$2\sqrt{2}\tau\sqrt{w} = \frac{1}{\sqrt{1-\rho}}.$$

Substituting in Equation (62) gives

$$\begin{aligned}\frac{d\mu}{d\rho}(w; h, \tau) &= -h\frac{\sqrt{\pi}}{2}\tau 2\sqrt{2}\tau\sqrt{w}\,\mathrm{e}^{-2w}\,\mathrm{e}^{w}\,\mathrm{I}_0(w)\\ &= -h\sqrt{2\pi}\tau^2\sqrt{w}\,\mathrm{e}^{-w}\,\mathrm{I}_0(w).\end{aligned}$$

From the NIST handbook (10.10.4), we have

$$\mathrm{I}_0(w) \sim \frac{\mathrm{e}^w}{\sqrt{2\pi w}} \quad w \to \infty. \tag{66}$$

Substituting this in the above, one finds, as $w \to \infty$,

$$\frac{d\mu}{d\rho}(w; h, \tau) \sim -h\sqrt{2\pi}\tau^2\sqrt{w}\,\mathrm{e}^{-w}\left(\frac{\mathrm{e}^w}{\sqrt{2\pi w}}\right) = -h\tau^2.$$

By the definition of w, there are three ways it can be made to become infinite: $\rho \to 1^-$, $\tau^2 \to 0$, or both. However, τ is a parameter and is held constant, so we take take $w \to \infty$ to be equivalent to $\rho \to 1^-$. Thus, the theorem is proven. □

3.2.5. Analysis of the Noncentrality Parameter

Now, we consider the mean in Equation (27) as a function of the noncentrality parameter λ.

Corollary 3. $\mu(\lambda; h)$*, given in Equation (39), is a decreasing function of* λ *over the interval* $(0, \infty)$.

Proof. For μ given in Equation (39) and with u and ψ defined in terms of λ as

$$u = \frac{1}{2}\frac{h^2}{\psi^2} \qquad\qquad \psi = \frac{h}{\lambda}$$

we can transform Equation (39) into the intermediate form. Combining these transformations, we see that $\lambda = \sqrt{2}\sqrt{u}$ and obtain

$$\mu(u; h) = h\frac{\sqrt{\pi}}{2}\frac{\mathrm{e}^{-u}}{\sqrt{u}}\,{}_1\mathrm{F}_1(3/2; 1; u). \tag{67}$$

Now, we proceed as before and use the properties of the intermediate form. By the chain rule,

$$\frac{d\mu}{d\lambda} = \frac{d\mu}{du}\frac{du}{d\psi}\frac{d\psi}{d\lambda}. \tag{68}$$

We note

$$\frac{d\psi}{d\lambda} = -h\psi^{-2}.$$

Using this with Equation (59) and Equation (50) in Equation (68) gives

$$\frac{d\mu}{d\lambda} = -h\frac{\sqrt{\pi}}{4}\frac{e^{-u}}{u^{3/2}}\,{}_1F_1(1/2;1;u)\left(-\frac{2u}{\psi}\right)\left(-\frac{h}{\lambda^2}\right). \tag{69}$$

Now, we use

$$\frac{1}{\sqrt{u}} = \frac{\sqrt{2}}{\lambda}$$

and

$$\frac{1}{\psi} = \frac{\lambda}{h}$$

to obtain

$$\frac{d\mu}{d\lambda}(\lambda;h) = -h\sqrt{\frac{\pi}{2}}\frac{e^{-\frac{\lambda^2}{2}}}{\lambda^2}\,{}_1F_1\left(1/2;1;\frac{\lambda^2}{2}\right). \tag{70}$$

From this, it is seen that $d\mu/d\lambda < 0$ by Lemma 1 over the interval $(0,\infty)$. Therefore, $\mu(\lambda;h)$ is decreasing. □

Corollary 4. *For $\mu(\lambda;h)$, given in Equation (39),*

$$\mu(\lambda;h) \sim h \tag{71}$$

as λ approaches ∞

Proof. It was just shown that under appropriate relationships among the parameters that $\mu(\lambda;h)$ can be transformed into the intermediate form $\mu(u;h) = h\Phi(u)$, where

$$u = \frac{1}{2}\lambda^2. \tag{72}$$

Undoubtedly $u \to \infty$ as $\lambda \to \infty$ and vice versa. Hence, we apply Theorem 2 and conclude that $\Phi(u) \sim 1$; therefore, $\mu(\lambda;h) \sim h$ as $\lambda \to \infty$. □

Now, we consider the derivative of the mean with respect to the noncentrality parameter.

Theorem 4. *For $\frac{d\mu}{d\lambda}(\lambda;h)$, given in Equation (70),*

$$\frac{d\mu}{d\lambda}(\lambda;h) \sim -\frac{h}{\lambda^3}$$

as $\lambda \to \infty$.

Proof. We change the variable to

$$t = \frac{\lambda^2}{4}$$

resulting in

$$\frac{d\mu}{d\lambda}(t;h) = -h\sqrt{\frac{\pi}{2}}\frac{e^{-2t}}{4t}\,{}_1F_1(1/2;1;2t). \tag{73}$$

As previously noted, the following relationship holds:

$$ {}_1\mathrm{F}_1(1/2;1;2t) = \mathrm{e}^t\,\mathrm{I}_0(t). \tag{74}$$

Using this in Equation (73) gives

$$\frac{d\mu}{d\lambda}(t;h) = -\frac{h}{4}\sqrt{\frac{\pi}{2}}\frac{\mathrm{e}^{-t}}{t}\,\mathrm{I}_0(t).$$

As seen in Equation (66), for $t \to \infty$,

$$\begin{aligned}\frac{d\mu}{d\lambda}(t;h) &\sim -\frac{h}{4}\sqrt{\frac{\pi}{2}}\frac{\mathrm{e}^{-t}}{t}\frac{\mathrm{e}^t}{\sqrt{2\pi t}}\\ &\sim -\frac{h}{8}\frac{1}{t^{3/2}}.\end{aligned}$$

Obviously, $t \to \infty$ if and only if $\lambda \to \infty$. Since $1/t^{3/2} = 8/\lambda^3$, we conclude that

$$\frac{d\mu}{d\lambda}(\lambda;h) \sim -\frac{h}{8}\frac{8}{\lambda^3} = -\frac{h}{\lambda^3} \tag{75}$$

as $\lambda \to \infty$. □

3.2.6. Analysis of the Scale Parameter

Now, we consider the influence of the τ parameter. Recall $\tau = \sigma/h$, which is the ratio of the spread of the fixation points to the height of the bar. It gives the scale of the visualization problem. Let us consider the sensitivity of the mean to it.

Corollary 5. *$\mu(\tau;h,\rho)$, given in Equation (38), is an increasing function of τ over the interval $(0,\infty)$.*

Proof. Using u and ψ satisfying

$$u = \frac{1}{2}\frac{h^2}{\psi^2} \qquad\qquad \psi^2 = 2h^2\tau^2(1-\rho)$$

then $\mu(\tau;h,\rho)$ can be transformed into the intermediate form in a fashion identical to what has already be done for $\mu(\rho;h,\tau)$.

By the chain rule,

$$\frac{d\mu}{d\tau} = \frac{d\mu}{du}\frac{du}{d\psi}\frac{d\psi}{d\tau}. \tag{76}$$

We need $d\psi/d\tau$:

$$\frac{d\psi}{d\tau} = \frac{d}{d\tau}(\sqrt{2}h\tau\sqrt{1-\rho}) = \sqrt{2}h\sqrt{1-\rho}. \tag{77}$$

Using Equation (77), Equation (59), and Equation (50) in Equation (76) gives

$$\frac{d\mu}{d\tau} = -h\frac{\sqrt{\pi}}{4}\frac{\mathrm{e}^{-u}}{u^{3/2}}\,{}_1\mathrm{F}_1(1/2;1;u)\left(-\frac{2u}{\psi}\right)(\sqrt{2}h\sqrt{1-\rho}).$$

We must eliminate u and ψ from the expression, leaving the parameters h and ρ. To this end, we transform it according to

$$\frac{1}{\psi} = \frac{1}{\sqrt{2}h\tau\sqrt{1-\rho}} \qquad\qquad \frac{1}{\sqrt{u}} = 2\tau\sqrt{1-\rho}.$$

After making the appropriate substitutions followed by basic manipulations, we obtain

$$\frac{d\mu}{d\tau}(\tau;h,\rho) = h\sqrt{\pi}\sqrt{1-\rho}\,\mathrm{e}^{-\frac{1}{4\tau^2(1-\rho)}}\,{}_1\mathrm{F}_1\left(1/2;1;\frac{1}{4\tau^2(1-\rho)}\right). \tag{78}$$

From this, it is seen that $d\mu/d\tau > 0$ by Lemma 1 over the interval $(0,\infty)$. Therefore, $\mu(\tau;h,\rho)$ is increasing. □

Corollary 6. *For $\mu(\tau;h,\rho)$, given in Equation (38),*

$$\mu(\tau;h,\rho) \sim h \tag{79}$$

as $\tau \to 0^+$.

Proof. As has already been demonstrated for $\mu(\rho;h,\tau)$, it is possible to transform this expression into the intermediate form. The details are seen in Corollary 1 and shall be omitted here.

Once $\mu(\tau;h,\rho)$ is transformed into $\mu(u;h) = h\Phi(u)$, we note that, unlike the other key parameters, as it becomes small, u becomes large, as can be seen from the definition

$$u = \frac{1}{4}\tau^{-2}\frac{1}{1-\rho}. \tag{80}$$

That is, $u \to \infty$ as $\tau \to 0^+$ and vice versa as ρ is a parameter that is held constant. Hence, Theorem 2 yields $\Phi(u) \sim 1$, and therefore, $\mu(\tau;h,\rho) \sim h$. □

Finally, we calculate the derivative with respect to τ and look at its asymptotic properties, as has been done similarly before.

Theorem 5. *For $\frac{d\mu}{d\tau}(\tau;h,\rho)$, given in Equation (78),*

$$\frac{d\mu}{d\tau}(\tau;h,\rho) \sim 2h(1-\rho)\tau \tag{81}$$

as $\tau \to 0^+$.

Proof. We change the variables to

$$v = \frac{1}{8\tau^2(1-\rho)}. \tag{82}$$

Substituting Equation (82) into Equation (78), we obtain

$$\frac{d\mu}{d\tau}(v;h,\rho) = h\sqrt{\pi}\sqrt{1-\rho}\,\mathrm{e}^{-2v}\,{}_1\mathrm{F}_1(1/2;1;2v). \tag{83}$$

Again, we have

$${}_1\mathrm{F}_1(1/2;1;2v) = \mathrm{e}^{v}\,\mathrm{I}_0(v)$$

which we use in Equation (83):

$$\frac{d\mu}{d\tau}(v;h,\rho) = h\sqrt{\pi}\sqrt{1-\rho}\,\mathrm{e}^{-v}\,\mathrm{I}_0(v).$$

Recalling the asymptotic behavior of the modified Bessel function given in Equation (66) and substituting into the previous equation, we obtain

$$\begin{aligned}\frac{d\mu}{d\tau}(v;h,\rho) &\sim h\sqrt{\pi}\sqrt{1-\rho}\,\mathrm{e}^{-v}\,\frac{\mathrm{e}^{v}}{\sqrt{2\pi v}}\\ &\sim \frac{h}{\sqrt{2}}\frac{1}{\sqrt{v}}\sqrt{1-\rho}\end{aligned}$$

as $v \to \infty$. We invert the mapping from v to τ using

$$\frac{1}{\sqrt{v}} = 2\sqrt{2}\tau\sqrt{1-\rho}.$$

Note that as $v \to \infty$, we have $\tau \to 0^{+}$

$$\begin{aligned}\frac{d\mu}{d\tau}(\tau;h,\rho) &\sim \frac{h}{\sqrt{2}}2\sqrt{2}\tau(1-\rho)\\ &\sim 2h(1-\rho)\tau.\end{aligned}$$

□

4. Discussion

A primary objective of this paper is to understand the so-called expected visual measurement error (EVME): that is, the mistakes people make when using the structure of the visualization to recover the number encoded in the height or length of a geometric mark. In particular, the error made in measuring the height of a bar in a bar graph.

There is no universally accepted definition of the expected visual measurement error, so this research proposes a simple one to explore it and see what can be learned. The definition of the EVME will be given in the next section. With a definition in hand, we can use all the extensive groundwork that has been prepared to explore its behavior.

Particular attention is given to the correlation parameter ρ, as this is a new contribution to this landmark literature. It can be said that there is no significance to such correlations if being applied to discovering the shape of a baboon's vertebrae, but we believe including the correlation is important, if not required, to model eye motion. It will be shown that the other parameters appear naturally in the analysis of the expected visual measurement error.

4.1. Expected Visual Measurement Error

Error is typically the difference between an actual and measured value. Knowing how the height of a bar is measured visually is problematic. This may be different person-to-person. Hence, we developed the approach for this course of work. Namely, we make the height of the bar a random variable. Let us work through the concept of this model.

First, the viewer looks at the base, leaving a fixation, then moves rapidly to the top of the bar (the next AOI). This is followed by a glance toward the ruler in an effort to obtain a reading on the height. The process is repeated by the path returning to the base of the bar to again obtain a feel for the height of the bar. This creates a family the forms a random triangle. See Figure 5. The circled edges are part of the height estimation process.

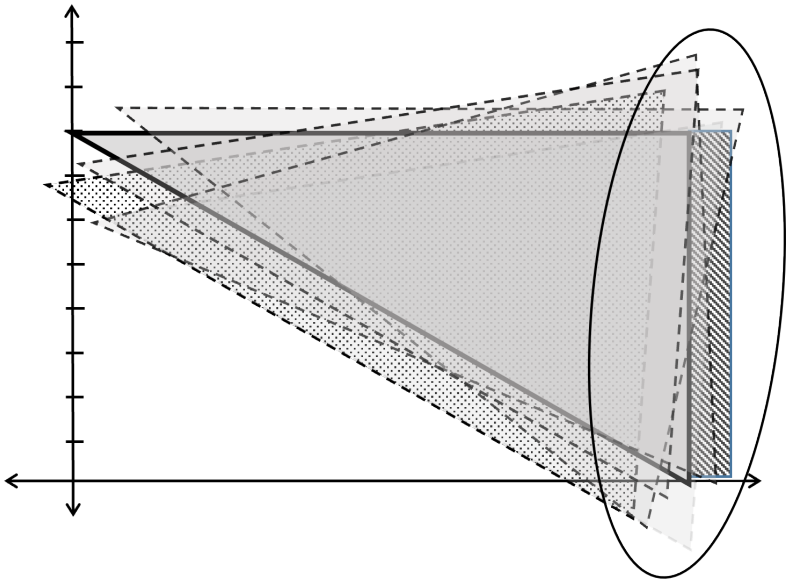


Figure 5. Conceptual view of the stochastic triangles connecting one fixation in each of the areas of interest. The circled edges have random lengths called D_{12} that possess an expected value called μ.

Figure 3 shows a particular triangle. The edge of the triangle $\mathbf{P_1P_2}$ has length D_{12}, which is a random variable with a noncentral chi distribution with noncentrality parameter λ, as has been discussed. The random variable is a model of the height of the bar. Admittedly, how the viewer uses the ruler to assign a length to D_{12} is not clear. From the model's perspective, each triangle would have associated with it a pairing $(r(\mathbf{P_3}), D_{12}(\mathbf{P_1}, \mathbf{P_2}))$, where $r(\mathbf{P_3})$ is the reading taken from the ruler based on vertex $\mathbf{P_3}$.

In this paper, it is proposed that after viewing the bar graph and creating multiple triangles, the viewer assigns the expected value of D_{12} as the measured height of the bar. (The exact mechanics of how this is done are not well explained. We envision that for each fixation by the ruler, a number is captured. This becomes the assigned length of the edge. In some sort of limiting process, the mean is recovered from an unbiased statistic. This is being actively investigated and will be an area of future publication.). That is, $r(\mathbf{P_3}) = E(D_{12})$. This makes the expected visual measurement error

$$\text{EVME} = \text{E}(D_{12} - h) = \text{E}(D_{12}) - h. \tag{84}$$

This brings us to the following key theorem.

Theorem 6. *For μ, given in Equation (27),*

$$\text{EVME} = (\text{E}(D_{12}) - h) \sim h(1-\rho)\tau^2 + \frac{1}{2}h(1-\rho)^2\tau^4 + \cdots \tag{85}$$

as $\tau \to 0^+$.

Proof. We appeal to the paper by Parks [29] for the formula for the asymptotic expansion of the mean as the noncentrality parameter becomes large. In his formula in the paper, we set $a = 1$ for the first moment, $N = 2$ for the number of degrees of freedom, and $y_0 = \lambda$ for the noncentrality parameter. This yields, after simplification,

$$\begin{aligned} \text{E}\left(\frac{D_{12}}{\psi}; \lambda\right) &\sim \lambda\left[1 + \frac{1}{2}\lambda^{-2} + \frac{1}{8}\lambda^{-4} + \cdots\right] \quad \lambda \to \infty \\ &\sim \lambda + \frac{1}{2}\lambda^{-1} + \frac{1}{8}\lambda^{-3} + \cdots \quad \lambda \to \infty \end{aligned}$$

so that

$$\mathrm{E}(D_{12}) \sim \psi\lambda + \frac{1}{2}\psi\lambda^{-1} + \frac{1}{8}\psi\lambda^{-3} + \cdots \quad \lambda \to \infty.$$

Now, we use $\lambda = h/\psi$:

$$\begin{aligned}\mathrm{E}(D_{12}) &\sim \psi(h/\psi) + \frac{1}{2}\psi(h/\psi)^{-1} + \frac{1}{8}\psi(h/\psi)^{-3} + \cdots \quad \tau \to 0^{+} \\ &\sim h + \frac{1}{2}(\psi^2/h) + \frac{1}{8}(\psi^4/h^3) + \cdots \quad \tau \to 0^{+}\end{aligned}$$

where $\tau = 1/\lambda$. We substitute $\psi^2 = 2h^2\tau^2(1-\rho)$ and rearrange terms to obtain

$$\mathrm{E}(D_{12}) - h = \mathrm{E}(D_{12} - h) \sim h\tau^2(1-\rho) + \frac{1}{2}h\tau^4(1-\rho)^2 + \cdots \quad \tau \to 0^{+}. \tag{86}$$

Therefore, we conclude

$$\mathrm{EVME} \sim h\tau^2(1-\rho) + \frac{1}{2}h\tau^4(1-\rho)^2 + \cdots \quad \tau \to 0^{+}. \tag{87}$$

□

This is a remarkable expression. It shows the higher-order dependency of the expected visual measurement error in terms of the parameters we have been studying. That the quality of the estimate should depend on τ was already suspected in the literature. Now that dependency is clearly seen. Before we study this matter and others, it is worthwhile to summarize what we have learned in our analysis of the basic parametric dependence of the mean.

4.2. Remarks on the Correlation Parameter

One of the main contributions of this paper is the analysis of the influence of the correlation. Let us look at it more closely. Recall that the general model originally proposed had seven correlations in it. In order to proceed, we had to consider cases that were tractable with the available mathematical machinery. Hence, we made decisions that uncorrelated η and ζ and give them identical variances. In particular, we set

$$\rho = \rho_1 = \rho_2 = \rho_{12x} = \rho_{12y} = \rho_{1y2x} = \rho_{1x2y}$$

with

$$\sigma = \sigma_{1x} = \sigma_{2x} = \sigma_{1y} = \sigma_{2y}$$

making $Cov(\eta, \zeta) = 0$ (see Equation (17) and $\psi = 2\sigma^2(1-\rho)$, which has allowed interesting analysis, but notice what happened in particular. Making $Cov(\eta, \zeta) = 0$ essentially removed four correlations from the model: namely, ρ_1, ρ_2, ρ_{1y2x}, and ρ_{1x2y}. The two correlations that remained in the model under the name of ρ were ρ_{12x} and ρ_{12y}. Furthermore, we required them to have the same sign and magnitude.

Figure 6 visualizes the consequences of the assumption we made regarding the correlation. Consider situations for which

$$\mathrm{corr}(d_{2x}, d_{1x}) = \mathrm{corr}(d_{2y}, d_{1y}) > 0.$$

This corresponds to fixation clouds that are either shifted to the right and up or to the left and down. Since we have assumed

$$\sigma = \sigma_{1x} = \sigma_{2x} = \sigma_{1y} = \sigma_{2y}, \tag{88}$$

the fixation clouds have roughly similar shapes at each end of the bar. This results in what is essentially a rigid body shift of the bar without a significant change of length. This is not the case with negative correlation. As shown in Figure 6, the fixation cloud shifts rotate the bar and either compress or stretch it.

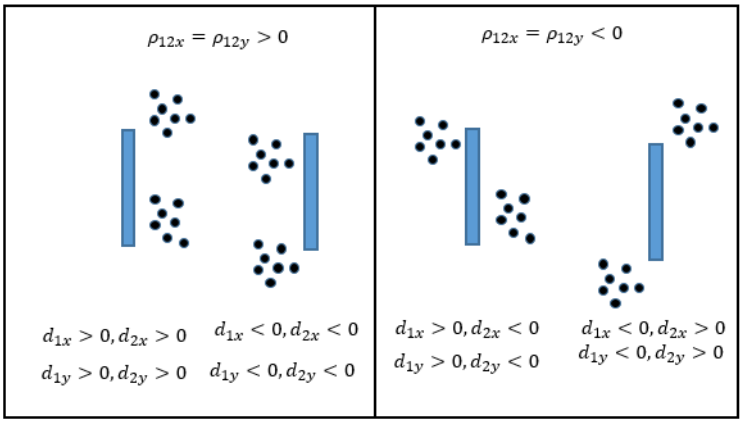


Figure 6. A visualization of the various cases surrounding values of the correlation.

Does the model support these suspicions? Recall Corollary 1 that shows the mean is decreasing for ρ over the interval $(-1, 1)$. The mean is the largest for fixation clouds with correlations near -1. This means the expected visual measurement error will be worse for negative correlations. This seems to be consistent with the foregoing discussion. Similarly, translations with little to no dilation would change the mean little. These correspond to strongly positive correlations. Furthermore, we know from Corollary 2 that $\mu \sim h$ as $\rho \to 1^-$, so the EVME will become small as the correlation becomes strongly positive. This would seem to be consistent with the previous observations shown in Figure 6.

What remains to question is whether there is a significant difference caused by including the correlation. We have calculated the derivative of the mean with respect to the correlation in Equation (62). Furthermore we know that as $\rho \to 1^-$,

$$\frac{d\mu}{d\rho} \sim -h\tau^2. \tag{89}$$

As we normally consider small values of τ, this says the derivative in these cases is small, particularly since τ is squared. Therefore, for positive correlation, there might not be much gained by including this parameter. However, for negatively correlated fixations, the relative size of the derivative is unknown.

4.3. Remarks on the Scale Parameter

The term τ has proven to be an important parameter. We know from Corollary 5 that the mean value of the random variable D_{12} is increasing in τ. This means that the mean is decreasing as τ approaches zero positively. Furthermore, Corollary 6 shows the mean asymptotically approximates h as $\tau \to 0^+$. From this, it follows that the expected visual measurement error is very small when τ is small.

It is reasonable to explore how the mean behaves as $\tau \to 0^+$. We found

$$\frac{d\mu}{d\tau} \sim 2h\tau(1-\rho). \tag{90}$$

This suggests that $\mu(\tau)$ is approximately quadratic in τ as it becomes small. We have already seen this in Equation (87), which was derived in a different manner. We provide more on this in the next section.

The need for small $\tau = \sigma/h$ is pervasive across the literature. In their book [23], Stoyan and Stoyan address the topic several times in a variety of settings, but mostly concerning the quality of statistical estimators. Anderson observes [31,32], for instance, that if $\sigma \ll h$, simple empirical estimators are as good as more complex maximum likelihood estimators. It should be noted that they often use a slightly different τ: namely, σ divided by the triangle's longest side, which is d_{13}. This affects the parametric analysis in interesting ways but will be saved for a future line of work.

Since we have keen interest in the correlation, we notice the role ρ plays. Strongly positive correlation will diminish the effects of scale on the mean, whereas strong negative correlation increases the effects of τ. Recall the interpretation that positive correlation results in less change in D_{12} and more rigid displacement. It seems reasonable that there would be less change in μ as τ changes, as indicated in asymptotic Equation (90). However, negative correlation was reasoned to be associated with a potentially greater length change. Therefore, $\mu(\tau)$ having a steeper slope near zero indicates greater change is happening.

The term τ is the parameter that ties the viewer and the visualization together. And σ is a property of the fixations and their spread about the ends of the bar. The term h is a property of visualization. The ratios of their values determine the quality of the visual assessment of the bar. In studies of figure shapes (which can be subdivided into sets of triangles if needed), τ is estimated [33,34]. This questions whether h and σ can be individual, separate parameters, or is their ratio intrinsic to the viewer? That is, will a viewer increase σ as h increases to keep some unstated value of τ constant? This seems like an interesting question for future experimental research.

4.4. Interesting Relationships

We have defined the expected visual measurement error as the expected value of the difference between the height of the bar and the length of a side of a stochastic triangle and found an asymptotic expansion for it:

$$\text{EVME} = \text{E}(D_{12} - h) = \text{E}(D_{12}) - h \sim h(1-\rho)\tau^2 + \frac{1}{2}h(1-\rho)^2\tau^4 + \cdots \tag{91}$$

as $\tau \to 0^+$. A few final observations are in order. Recall Equation (64):

$$\frac{d\mu}{d\rho} \sim -h\tau^2 \tag{92}$$

as $\rho \to 1^-$. If we take the partial derivative of the EVME in Equation (91) with respect to ρ and keep the term to the lowest order, we have

$$\frac{\partial \text{EVME}}{\partial \rho} \sim -h\tau^2.$$

(These are just formal manipulations. In order to be able to take derivatives of asymptotic expansions, certain conditions must hold [35]. Our purpose is just to make a casual observation, not to prove a rigorous result.)

Similarly, we have from Equation (81) that

$$\frac{d\mu}{d\tau}(\tau; h, \rho) \sim 2h(1-\rho)\tau.$$

If this time we formally take the partial derivative of the expected visual measurement error with respect to τ, we have

$$\frac{\partial \text{EVME}}{\partial \tau} \sim 2h(1-\rho)\tau.$$

The significance of this is that these relations were reached from two different directions. In one direction, the derivatives of the mean were calculated directly and the asymptotic properties of the Bessel functions were used to reach the asymptotic approximations. In the other direction, Park used the asymptotic expansion of the confluent hypergeometric function found in [36], then we took the derivative of it. This process could have easily failed. That it did not suggests there is an internal consistency to what has been developed.

5. Conclusions

The purpose of this paper was to develop estimations of the expected error in reading a bar graph. This estimate was a consequence of a mathematical model we constructed of the decoding process based upon concepts within eye tracking. With this accomplished, several questions are encountered. To what extent can this model be adapted to other visualizations? What are its limitations? How can it be applied, and what work remains to be done?

5.1. Limitations of the Model

If handed a dataset and a visualization, a reasonable question is whether the model can be adapted to provide error estimates in the decoding process of the visualization. To answer that, we would first look to see if the visualization represents numeric data. That is a requirement. Next, we would consider how many measurements must be made to decode the data value. A bar graph is one measurement, and this is what the model simulates in its current state. We say this is one-dimensional since there is one measurement. A line chart is two measurements—one for the x coordinate and one for the y coordinate; we call this two-dimensional. Finally, we would inquire which elementary task must be performed to decode that number.

It is worthwhile to review the elementary perceptional tasks as categorized by Cleveland and McGill [3]. They identified 10 ways by which a number can be encoded in a visualization. They performed a series of experiments and were able to group the tasks together by how accurately the encoded number could be extracted. They produced six groups.

As can be seen from Table 1, there are three elementary perceptual tasks for which it is believed the model could be applied, three that present research challenges, and four that are simply beyond the model. This allows us to make some basic lists of visualizations that could work with a modified model and a list of those that are beyond the boundaries of the model.

Table 1. Elementary perceptional tasks ordered by accuracy.

Elementary Task	Ordering	Model Can Interpret This Task
Position along a common scale	1	Yes. 1-dimensional length measure.
Positions along nonaligned scales	2	Yes. 1-dimensional length measure.
Length	3	Yes. 1-dimensional length measure.
Direction	3	No, for now.
Angle	3	No, for now.
Area	4	Maybe.
Volume	5	No.
Curvature	5	No.
Shading	6	No. Model is blind to shading.
Color Saturation	6	No. Model is colorblind.

Let us look at some common visualizations that are outside of the boundaries of the model we built. A favorite chart for people that is beyond this model is the pie chart, which depends upon angles to encode its numeric values. A pie chart is just a bar graph mapped onto the polar coordinate system, but that passage from linear (or rectangular) to radial (or circular) challenges the effectiveness of the stochastic model developed herein. Almost

any visualization based on a polar grid is beyond the limitations of this model. These include: radial bar charts, donut charts, polar area charts, radial histograms, radial line charts, multilevel pie charts, spiral histograms, and so forth.

It should also be noted that the model does not fit relational data: that is, that two people are friends or brother/sister. Any of the relational charts are beyond it: graphs, digraphs, weighted digraphs, arc diagrams, trees, chord diagrams, non-ribbon chord diagrams, etc.

5.2. Extensions to Other Visualization Types

Before proceeding, it is important to note that this paper developed a model from which various things were learned and an error estimate produced. It did not produce a method. A method is a tool that could be used on other visualizations. A model is a house built on a foundation (visualization). It has rooms, attributes, and characteristics and provides certain functionality for us. Taking the results of this paper and trying to apply them to a different type of visualization means the house must be built again. The more analogous the new visualization is to a bar graph, the simpler the construction of the new house. The less a visualization resembles a bar graph, the more effort will have to go into building the model for that visualization. In time, perhaps we will have a "general model" that covers a variety of visualizations without the need for reproof. However, this paper was a first step in showing the model exists and has some use for a bar graph.

Now let us consider some extensions. The strip plot is a one-dimensional scatter plot (see Figure 7). The data are numeric. There is only one measurement required, and finding a position along an aligned axis is the perceptional task. The geometry is linear. Once a point is picked, the problem of reading the coordinate on the axis is very similar to that of a bar chart. It looks like a good candidate for a successful build of our model. From a certain perspective, it is a many-valued bar chart. How that might impact the analysis would be interesting to see.

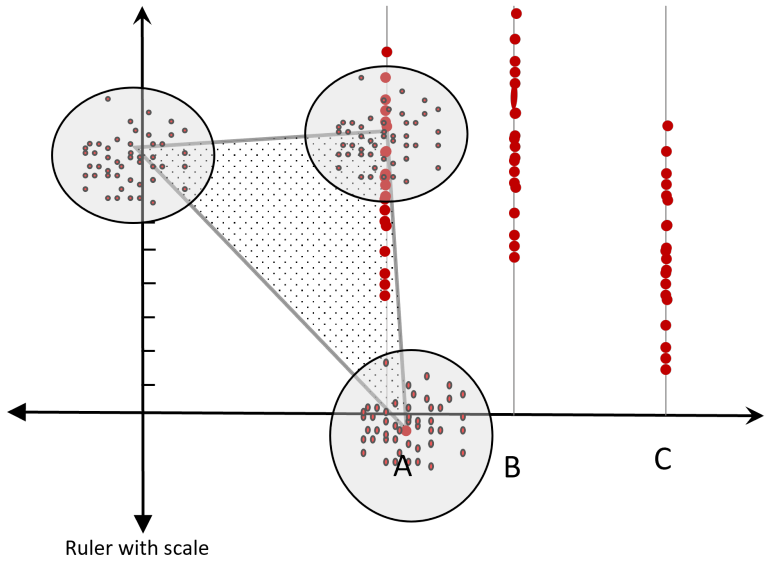


Figure 7. The fundamental stochastic triangle on a strip plot.

A step up in complexity is the line graph, which has the same triangular structure when reading the coordinates of a point as a bar graph (See Figure 8). We place one AOI over the point. We drop down vertically and place an AOI over the x coordinate and cross horizontally to cover the y coordinate. In this case, there are two estimates: one for x and one for y, which differs from the bar graph. This capability to estimate two lengths is in this model. The random triangle that is constructed has three sides that we can utilize for length estimation. Our intuition is that for the analysis to extend, it would be necessary

for the (x, y) pairs to be sufficiently spaced so that a reasonable AOI contains only one data point.

A scatter plot is a step up in complexity over the line graph. The reason is that there may be multiple data points in the AOIs. This will make the analysis to build the model more complex.

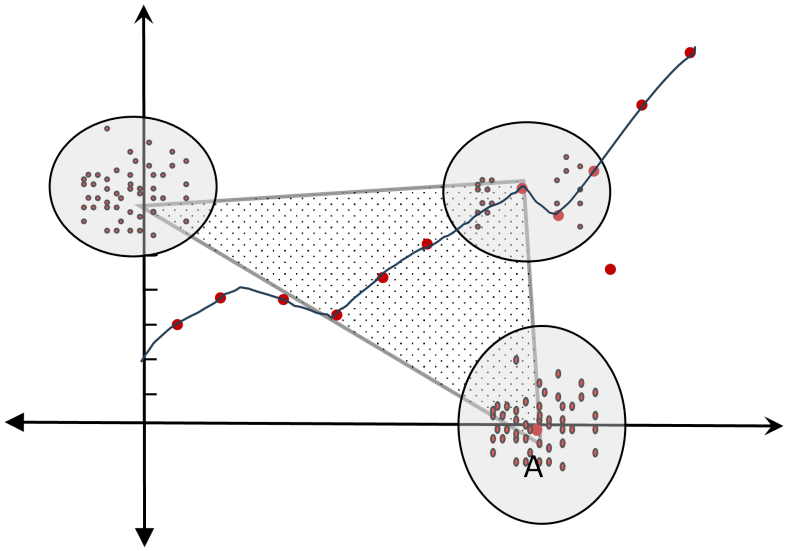


Figure 8. The fundamental stochastic triangle on a line graph.

Putting this together, then natural visualizations open to models similar to the one developed herein also include vertical bar graphs, horizontal bar graphs, line charts, time series, scatter plots, and so forth. Requiring the visualization to have equal salience means that coloring or shading cannot be used to distinguish levels of categorical variables. Hence, a stacked bar chart, as well as a clustered bar chart, etc., is currently out of the boundaries of the model.

5.3. Applications

While eye-tracking concepts permeate the development of this model, its application has nothing to do with eye tracking. The purpose of the model is to produce an expected error inherent in reading a bar graph. That is, anyone reading a bar graph may be expected to experience an expected error of the amount of the EVME. Keep in mind, however, that the EVME is an expected value, so it is an average of user behavior. Some people may accurately read the graph; others will be less accurate. The amount of error, on average, will be about the EVME. Ideally, visualization designers could attempt to minimize the EVME for a particular chart in order to produce more reliable reading of the data.

Recalling Equation (85) to the lowest order in τ,

$$\text{EVME} = (\text{E}(D_{12}) - h) \sim h(1-\rho)\tau^2 + \cdots$$

as $\tau \to 0^+$. Here, we see that the expected error is approximately the product of three parametric expressions. The term h is the height of the bar and is under the control of the designer, and ρ is due to the eyes of the viewer and how they correlate in adjacent AOIs. For discussion purposes, let us suppose that there is no correlation. That is, $\rho = 0$. Then

$$\text{EVME} = (\text{E}(D_{12}) - h) \sim h\tau^2 + \cdots$$

Suppose we can hold τ small but constant while changing h. Then this shows us that designers should avoid longer bars for that scaled visualization. With that said, we must confront the issue of whether we can increase h while holding τ constant, since $\tau = \sigma/h$.

Will the fixation variation naturally adjust to compensate for the larger h? It seems possible that the more isolated the bar is from other bars, the tighter the point cloud of fixations will group around the tip of the bar. If the bars are tightly grouped, then eye fixations may involve other bars, creating a larger variation and, thereby, increasing σ. This suggests that τ can be controlled by the designer; however, it will likely take experimentation to understand the nature of this dependency.

Allowing for $\rho \neq 0$ means that the correlation influences the EVME. The nature of this dependency has been discussed in the previous section. We observed that negative correlations can increase the EVME up to a factor of two times. This is the first research to include correlation in this fashion, so how it can be controlled is still open. However, it might account for unexplained error in a particular visualization design.

5.4. Future Work

This paper is the first step down a path requiring further theoretical development and experimental exploration. As is true in most scientific investigation, these are coupled together. It is our intention to pursue both.

On the theoretical side, we need to have error estimates for the side called D_{23}, which is originally of length b and is the distance of the bar from the vertical axis. This will show the influence b has on visualization design and error in reading the height of the bar. It would seem that the further the bar is from the axis, the greater the EVME would be. This has yet to be established.

Experimentally, there are several items to explore. Of course, the most basic experiment is to vary the bar height and record the accuracy of the reading. This would need to be repeated for several test subjects and averaged to obtain an approximate expected value curve of error vs. height. It should be approximately linear.

The problem in doing this is that the different visualizations may have different values of τ. This means a more complete experimental investigation of scale is required. Fortunately, this has been much-studied in landmark theories from stochastic geometry, so there is a rich statistical foundation upon which we can apply these ideas to visualizations.

The correlation parameter is new to this setting. There is no established analogy in landmark theories, so this will require further investigation to obtain the proper statistics and testing to see if the design of the visualization influences the correlated movement of the eye.

In conclusion, the work has presented a novel approach to error analysis of the decoding process of numerical bar graphs. While it is only the beginning, further theoretical and experimental investigation may open the door to a broader setting and a deeper understanding of visualization interpretation.

Funding: This research received no external funding.

Institutional Review Board Statement: Not applicable.

Data Availability Statement: The original contributions presented in the study are included in the article, further inquiries can be directed to the corresponding author.

Acknowledgments: The author wishes to acknowledge the Department of Business and Information Technology, which provided funds for the purchase of research books relevant to this project.

Conflicts of Interest: The author declares no conflicts of interest.

Abbreviations

The following abbreviations are used in this manuscript:

AOI	area of interest
pdf	probability density function
EVME	expected visual measurement error

References

1. Tufte, E.R. *The Visual Display of Quantitative Information*, 2nd ed.; Graphics Press: Cheshire, CT, USA, 2001.
2. Michalos, M.; Tselenti, P.; Nalmpantis, S. Visualization Techniques for Large Datasets. *J. Eng. Sci. Technol. Rev.* **2012**, *5*, 72–76. [CrossRef]
3. Cleveland, W.S.; McGill, R. Graphical perception: Theory, experimentation, and application to the development of graphical methods. *J. Am. Stat. Assoc.* **1984**, *79*, 531–554. [CrossRef]
4. Heer, J.; Bostock, M. Crowdsourcing graphical perception: Using mechanical turk to assess visualization design. In Proceedings of the SIGCHI Conference on Human Factors in Computing Systems, Atlanta, GA, USA, 10–15 April 2010; pp. 203–212.
5. Shah, P.; Hoeffner, J. Review of graph comprehension research: Implications for instruction. *Educ. Psychol. Rev.* **2002**, *14*, 47–69. [CrossRef]
6. Connor, C.E.; Egeth, H.E.; Yantis, S. Visual attention: Bottom-up versus top-down. *Curr. Biol.* **2004**, *14*, R850–R852. [CrossRef]
7. Pinto, Y.; van der Leij, A.R.; Sligte, I.G.; Lamme, V.A.; Scholte, H.S. Bottom-up and top-down attention are independent. *J. Vis.* **2013**, *13*, 16. [CrossRef]
8. Matzen, L.E. *Using Eye Tracking Metrics and Visual Saliency Maps to Assess Data Visualizations*; Technical Report; Sandia National Lab.(SNL-NM): Albuquerque, NM, USA, 2016.
9. Matzen, L.E.; Haass, M.J.; McNamara, L.A. *Using Eye Tracking to Assess Cognitive Biases*; Technical Report; Sandia National Lab.(SNL-NM): Albuquerque, NM, USA, 2014.
10. Borkin, M.A.; Vo, A.A.; Bylinskii, Z.; Isola, P.; Sunkavalli, S.; Oliva, A.; Pfister, H. What makes a visualization memorable? *IEEE Trans. Vis. Comput. Graph.* **2013**, *19*, 2306–2315. [CrossRef]
11. Jacob, R.J.; Karn, K.S. Eye tracking in human-computer interaction and usability research: Ready to deliver the promises. In *The Mind's Eye*; Elsevier: Amsterdam, The Netherlands, 2003; pp. 573–605.
12. Rayner, K. Eye movements in reading and information processing: 20 years of research. *Psychol. Bull.* **1998**, *124*, 372. [CrossRef]
13. Rayner, K. Eye movements and attention in reading, scene perception, and visual search. *Q. J. Exp. Psychol.* **2009**, *62*, 1457–1506. [CrossRef]
14. Higgins, E.; Leinenger, M.; Rayner, K. Eye movements when viewing advertisements. *Front. Psychol.* **2014**, *5*, 210. [CrossRef]
15. Harel, J.; Koch, C.; Perona, P. Graph-based visual saliency. In Proceedings of the 19th International Conference on Neural Information Processing Systems (NIPS'06), Vancouver, BC, Canada, 4–7 December 2006; MIT Press: Cambridge, MA, USA, 2006.
16. Matzen, L.E.; Haass, M.J.; Tran, J.; McNamara, L.A. *Using Eye Tracking Metrics and Visual Saliency Maps to Assess Image Utility*; Technical Report; Sandia National Lab.(SNL-NM): Albuquerque, NM, USA, 2016.
17. Haass, M.J.; Matzen, L.E.; Butler, K.M.; Armenta, M. A new method for categorizing scanpaths from eye tracking data. In Proceedings of the Ninth Biennial ACM Symposium on Eye Tracking Research & Applications, Charleston, SC, USA, 4–17 March 2016; pp. 35–38.
18. Collewijn, H.; Erkelens, C.J.; Steinman, R.M. Binocular co-ordination of human horizontal saccadic eye movements. *J. Physiol.* **1988**, *404*, 157–182. [CrossRef]
19. Collewijn, H.; Erkelens, C.J.; Steinman, R.M. Binocular co-ordination of human vertical saccadic eye movements. *J. Physiol.* **1988**, *404*, 183–197. [CrossRef]
20. Bahill, A.T.; Stark, L. Oblique saccadic eye movements: Independence of horizontal and vertical channels. *Arch. Ophthalmol.* **1977**, *95*, 1258–1261. [CrossRef]
21. Bookstein, F.L. Size and shape spaces for landmark data in two dimensions. *Stat. Sci.* **1986**, *1*, 181–222. [CrossRef]
22. Goldberg, J.; Helfman, J. Eye tracking for visualization evaluation: Reading values on linear versus radial graphs. *Inf. Vis.* **2011**, *10*, 182–195. [CrossRef]
23. Stoyan, D.; Stoyan, H. *Fractals, Random Shapes and Point Fields: Methods of Geometrical Statistics*; John Wiley & Sons Incorporated: Hoboken, NJ, USA, 1994; Volume 302.
24. Miller, K. Distributions involving norms of correlated Gaussian vectors. *Q. Appl. Math.* **1964**, *22*, 235–243. [CrossRef]
25. Miller, K.S. *Multidimensional Gaussian Distributions*; Wiley: Hoboken, NJ, USA, 1964.
26. Hilgers, M.G.; Burke, A. Exploring Errors in Reading a Visualization via Eye Tracking Models Using Stochastic Geometry. In *HCI in Business, Government and Organizations. Information Systems and Analytics, Proceedings of the 6th International Conference, HCIBGO 2019, Held as Part of the 21st HCI International Conference, HCII 2019, Orlando, FL, USA, 26–31 July 2019*; Proceedings, Part II 21; Springer: Cham, Switzerland, 2019; pp. 53–71.
27. Krishnaiah, P.; Hagis, Jr, P.; Steinberg, L. A note on the bivariate chi distribution. *SIAM Rev.* **1963**, *5*, 140–144. [CrossRef]
28. Lawrence, J. Moments of the noncentral chi distribution. *Sankhya A* **2021**, *85*, 1243–1259. [CrossRef]
29. Park Jr, J. Moments of the generalized Rayleigh distribution. *Q. Appl. Math.* **1961**, *19*, 45–49. [CrossRef]
30. Olver, F.W.; Lozier, D.W.; Boisvert, R.F.; Clark, C.W. *NIST Handbook of Mathematical Functions Hardback and CD-ROM*; Cambridge University Press: Cambridge, UK, 2010.
31. Anderson, D.A. Maximum likelihood estimation in the non-central chi distribution with unknown scale parameter. *Sankhyā Indian J. Stat. Ser. B* **1981**, *43*, 58–67.
32. Anderson, D.A. The circular structural model. *J. R. Stat. Soc. Ser. B (Methodol.)* **1981**, *43*, 131–141. [CrossRef]
33. Mardia, K.; Dryden, I. The statistical analysis of shape data. *Biometrika* **1989**, *76*, 271–281. [CrossRef]
34. Mardia, K.; Dryden, I. Shape distributions for landmark data. *Adv. Appl. Probab.* **1989**, *21*, 742–755. [CrossRef]

35. Olver, F. *Asymptotics and Special Functions*; CRC Press: Boca Raton, FL, USA, 1997.
36. Jahnke, E.; Emde, F. *Tables of Functions with Formulae and Curves*; Dover Publications: Mineola, NY, USA, 1945.

Disclaimer/Publisher's Note: The statements, opinions and data contained in all publications are solely those of the individual author(s) and contributor(s) and not of MDPI and/or the editor(s). MDPI and/or the editor(s) disclaim responsibility for any injury to people or property resulting from any ideas, methods, instructions or products referred to in the content.